MPHIL

Synthesis and modification of zeolite catalysts and an assessment of their activity in the hydrogenation of a model hydrothermal liquefaction (HTL) bio-oil

Cai, Junjun

Award date:
2016

Awarding institution:
University of Bath

Synthesis and modification of zeolite catalysts and an assessment of their activity in the hydrogenation of a model hydrothermal liquefaction (HTL) bio-oil

Junjun Cai

A thesis submitted for the degree of Master of Philosophy

University of Bath

Department of Chemical Engineering

October 2015

CONTENT

ACKNOWLEDGEMENTS

First of all, I would like to extend my sincere gratitude to my supervisors, Dr. Christopher Chuck, Dr. Asel Sartbaeva and Dr. Valeska Ting for their time, support and enthusiasms in my project. I am grateful for their suggestions and careful revision in my report writing and revising.

I would also like to thank all the people who have supported and helped me with my project, particularly technicians in both of chemistry and chemical engineering departments, PhD student Ka Ming Leung for his help with synthesis of zeolite, and Dr. Rhodri W. Jenkins for his help in conversion test equipment set up and results analysis. At the end, I would also like to thank Miss. Wu for her countless help and support personally.

Finally, I would like to acknowledge all the members in my research groups for your support and making my MPhil such a wonderful experience.

ABSTRACT

Bio-oils produced from the thermal processing of biomass will play a promising role in the replacement of conventional fuel reserves. One likely processing method is the hydrothermal liquefaction (HTL) of microalgae. However, despite being more stable than pyrolysis oils, the high acidity, high oxygen and high nitrogen content, restrict the oils performance, and as such need to be upgraded by catalytic hydrogenation. Porous structure catalysts, especially zeolites have been widely applied to pyrolysis bio-oil upgrading, though to date have not been investigated for the upgrading of HTL oils, or HTL oils produced from microalgae. To this end, the zeolite FAU, MOR and ZSM-5 were synthesized, ion-exchanged and well characterized to study their performance on the upgrading of bio-oils. Firstly, the FAU, MOR and ZSM-5 zeolite were synthesized. In the presence of sodium base, and the FAU and MOR were ion-exchanged by ammonia nitrite solution. After that, the FAU and MOR were calcined to remove the ammonia ions from structure. The catalysts were characterized via XRD, FTIR, SEM, EDX, BET and SS-NMR. All the results shows that the zeolites are follow the pattern from international zeolite association, and the Si/Al ratio of FAU, MOR and ZSM-5 are around 2, 7, and 16 respectively. Finally, all the catalysts were screened for their activity with a model oil, designed to mimic HTL algal bio-oils, under high temperature and 40 bar of hydrogen pressure. The catalyst performance was monitored by ^{1}H NMR. All the catalysts demonstrated some activity in hydrogenating dodecylamine and pyrazine, though despite ZSM-5 being widely used in the hydrogenation of pyrolysis bio-oils, it was the FAU zeolites that were the most active for this model HTL bio-oil. H-FAU achieved the highest reduction in pyrazine whereas NH_4-FAU was the most active catalyst for the hydrogenation of dodecylamine. This is presumably because FAU has a relatively high surface area and mesopores in its structures comparing to other type of zeolite synthesized and applied in this project. Interestingly, little activity was observed in the reduction of double bonds or aromatics in the model oil, this suggests that while the zeolites could be used to provide denitrogenation for an algal bio-oil, it seems likely that metal nanoparticles are necessary to fully hydrogenate these oils.

1 LITERATURE REVIEW

1.1 INTRODUCTON

With the rapid industrial development of the modern era, huge fossil energy consumption has led to wide scale environmental pollution. In addition supplies of fossil fuels are becoming scarcer leading to a critical problem in the future due to unrestrained population growth. Therefore, the development of sustainable energy and resources are important to future development. One suitable replacement for transport energy are biofuels produced from food crops and latterly biomass waste products.[1]

In order to meet industrial and civil needs, as well as reducing the burden on the environment, new pathways to sustainable biofuel production must be developed. First-generation biofuels use sugars and starches and other raw materials obtained from food crops, for instance, rapeseed oil, palm oil, sorghum and maize. These feedstocks are used to produce bioethanol from fermentation or through the transesterification of seed oil to produce biodiesel [2]. Bioethanol is most frequently used as an engine fuel or as a fuel additive. Brazil produces the highest level of bioethanol and gasoline sold in Brazil contains at least 25% of ethanol [3], though higher blend levels are obtainable in every forecourt. However, there is simply not enough land to meet global demand on energy through first-generation biofuels and there increased use could cause food shortages and even famine [4].

To solve this problem, second-generation biofuels have emerged. Second-generation biofuels are produced using non-food crops as a feedstock, which do not compete with arable land, these include straw, grass and wood, agricultural and forestry wastes as raw materials. For example, the biological conversion of cellulose to bioethanol is commonly known as cellulosic ethanol [2, 3]. Compared with the first generation biofuels, second-generation bioethanol has several advantages. Firstly, cellulosic bioethanol can be directly incorporated into the gasoline stream and does not behave differently to first generation bioethanol; secondly, the technology costs while large at present will decline rapidly as large-scale industrial production comes into the market. Thirdly, lignocellulosic materials are far more widespread and could make a large contribution to displacing fossil fuels [5]. However, bioethanol has a low energy density, can only be

used in limited blend levels and has a poor return on investment [2, 4].

An alternative is microalgae, a so-called third-generation feedstock. The use of microalgae would completely avoid the use of food crops or arable land and therefore reduce competition with food resources [6]. Compared with lignocellulosic materials, algae have a higher efficiency of photosynthesis, stronger environmental adaptability, shorter growth cycle (typically take months or even years for higher plants to complete a generation of growth, whereas algae can grow to maximum biomass in up to 7 days). Moreover, the optimal growth conditions can be automated and controlled. Algae can also be cultured on waste water, and as such algal farms could be located in water areas that are near the sources of polluting water, in this way, the algal growth would not only be optimized due to excessive nutrients but would aid in remediation of the waste water. Another advantage of algae as a biofuel feedstock is that it requires CO_2 to grow and therefore does not need lignocellulosic.[7]

Algae contain a relatively high lipid content, soluble polysaccharides and proteins, which are components easy to conduct thermal chemical conversion. Whereas, wood lignin and cellulose, the main component of lignocellulosic materials, are more difficult to break down. Therefore, algae require relatively milder thermal chemical conversion conditions [7]. However, one of the major drawbacks to microalgae biofuels are the low density in the supernatant water, which leads to expensive and energy intensive extraction issues [8].

Currently, microalgae has been transformed by different conversion processes into a range of biofuels, for instance, biodiesel, bioethanol, biosynthesis gas, bio-oil and bio-hydrogen. Currently the majority of studies on microalgal oil are focused on the production of biodiesel obtained from oleaginous microalgal species. Figure 1 illustrates the general different steps for biofuel production from microalgae [9].

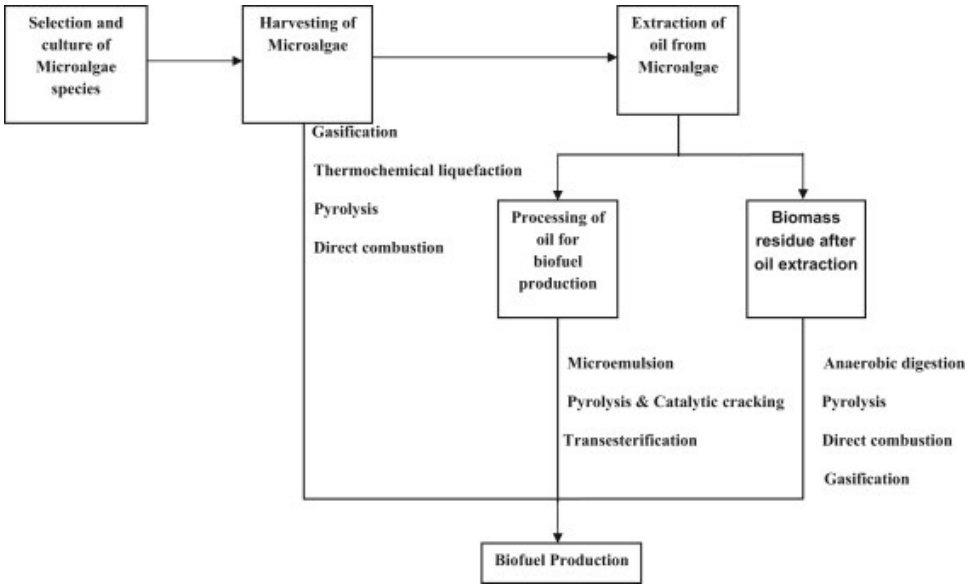

Figure 1 Different routes to biofuel production from microalgae, reproduced from [8].

Initially the algae are selected and harvested, then the algae undergo an extraction step to release the lipid. After this step the lipid is upgraded to biofuel via different methods, such as transesterification or catalytic cracking. The rest of biomass can be recycled to grow more algae.

However, the conventional pathway to produce biodiesel is not an ideal solution to produce biofuels since the speed of lipids grown is extremely slow and it is too expensive to extract the lipids from the algae [10].

1.2 THERMAL CHEMICAL PROCESS IN MICROALGAE

Microalgae biomass can be converted by a number of thermochemical methods, such as gasification and liquefaction into liquid fuels and other chemical products. In contrast to the biomass through gasification, liquefaction can directly produce liquid fuels in high yields. The direct liquefaction pathway can be achieved through pyrolysis or hydrothermal liquefaction (HTL) [11].

1.2.1 PYROLYSIS

Pyrolysis is a chemical process that converts biomass in an oxygen free atmosphere. It is generally conducted without a catalyst, at

around 500 °C. The components of pyrolysis bio-oils are extremely complex, [12] but mostly are made of oxygen-rich organic compounds. Typical compounds found are char, condensable organic liquids, acetic acid, acetone, methanol and non-condensable gases [9]:

Thermal chemical conversion of microalgae tends to obtain a high aromatic content, and high-octane value bio-oil. Studies have shown that, carbon and hydrogen content in microalgal bio-oil is higher than the lignin content material bio-oil and contains lower levels of oxygen, so the heating value of microalgal bio-oil is higher and relatively stable [13].

The compound distribution is related to the pyrolysis reaction temperature, heating rate, reaction time and other conditions, the pyrolysis process can be generally divided into fast and slow pyrolysis reactions. The main product of the slow pyrolysis is coke, and a by-product of bio-oil. While the main products of fast pyrolysis reaction are bio-oil and combustible gas with high conversion efficiency. Using fast pyrolysis as high as 80% of the biomass is converted to crude bio-oil [13]. Moreover, the speed of pyrolysis can influence the yield of bio-oil. For instance, the faster the pyrolysis rate is carried out, the more bio-oil is produced. Therefore, the most effective way to generate bio-oil via pyrolysis is via flash pyrolysis [9].

Before conducting the pyrolysis process, the biomass needs to be dried to the moisture of 7%. The dryers basically can be classified as two types direct dryer and indirect dryer. Most of commercial dryers applied in the pyrolysis process are direct dryers. There are two types of direct dryers air dryer and stream dryer can both reach the recommend moisture but they also have obvious disadvantages. For example, the air dryer has a potential fire hazard, which can cause severe safety issues during the process. For stream dryers, although it does not have a fire hazard, it requires extremely high capital costs. Moreover, stream dryers are very sensitive to the particle size, the feedstock needs to be parted to very small size to fit the dryer, which will also requires more costs on the biomass preparation.[9]

The cost of drying the algal biomass is thought to be prohibitively high, and while the bio-oils have an elevated performance compared to lignocellulose bio-oils they still cannot be used in conventional fossil fuel engines, since their high oxygen content, acidity and water content of the products are about 25-50 wt%. These properties can cause corrosion to the engines and make the oil unstable. Therefore, pyrolysis method is not a promising technology to convert biomass

into biofuels.[9]

1.2.2 HYDROTHERMAL LIQUEFACTION

An alternative reaction is Hydrothermal Liquefaction (HTL), which is potentially more energy efficient as there is no need to dewater the algae compared with the biodiesel production or pyrolysis methods discussed previously. HTL converts biomass into bio-oils in hot compressed water. Moreover, it is also an ideal method for conducting low-lipid-content microalgae with a very large amount of water since it uses the whole alga cell instead of oil extraction lipid [11]. Figure 2 indicates the basic process of hydrothermal liquefaction conversion, followed by chemical upgrading, of microalgae:

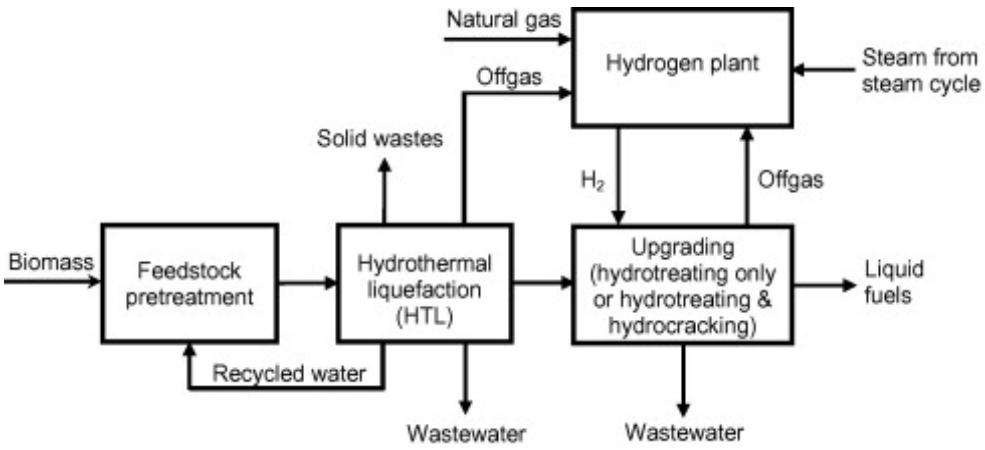

Figure 2 Schematic showing the conversion of biomass through HTL and the eventual upgrading. Adapted from [9].

For the HTL process, the microalgae conversion conditions range between 280°C, 10 MPa to 370°C, 25 MPa. Furthermore, the hydrothermal liquefaction process is generally followed by a catalytic upgrading reaction to achieve a high quality hydrocarbon fuel product [1].

The water used in the HTL process can also be replaced by a range of reactive organic solvents. For instance, ethanol is a commonly used replacement. Compared with water, ethanol has several advantages: (1) it reacts with acidic components to produce diesel-like products, (2) it dissolves high-molecular-weight liquid products to prevent coke formation, (3) ethanol stabilizes the free radicals to reduce the repolymerization reaction because of its hydrogen donor capability, and (4) it provides milder reaction conditions because its critical temperature and pressure are much lower [14].

However, using pure ethanol will cause a significant increase in energy cost and increases yields of sediment especially under high loadings [14]. Primarily however the advantage of not having to dry the algae is lost.

HTL reactions take place at a range of conditions and the product distribution changes with temperature, pressure and reaction duration. The HTL reaction is a complicated environment which multiple reactions taking place, for instance, depolymerization, fragmentation, dehydration, and decarboxylation [11]. Table 1 shows the main components of the bio-oil produced by HTL of microalgae.

Table 1 Major components of HTL bio-oil produced with ethanol and water co-solvent, where R represents the ratio of ethanol and water mass. Reproduced from [13].

	Peak area (%)[a]		
	R=5:2	R=1:1	R=2:5
Ketones	41.95	61.77	58.69
3-penten-2-one, 4-methyl	18.08	32.24	27.56
2-pentanone, 4-hydroxy-4-methyl	21.24	28.55	29.73
2-pentanone, 4-amino-4-methyl	1.44		
2-cyclopenten-1-one, 2,3-dimethyl	1.19	0.98	1.40
Esters	28.45	17.18	7.27
Hexadecanoic acid, ethyl ester	13.64	8.07	3.62
Octadecanoic acid, ethyl ester	1.76	1.15	0.42
Linoleic acid, ethyl ester	7.86	6.03	2.27
Nitrogen-containing heterocyclic compounds	24.66	19.68	30.14
1H-pyrrole, 3-ethyl-2,4,5-trimethyl	5.68	5.47	7.02
Pyrazine, methyl	1.15	2.43	1.89
4-piperidinone, 2,2,6,6-tetramethyl	12.83	5.41	16.35
Pyrrolo[1,2-a]pyrazine-1,4-dione, hexahydro-3-(phenylmethyl)		1.15	
Hydrocarbons	3.61	0.88	2.97
Cyclopentene, 1-hexyl	2.47	0.27	1.90
(2E)-3,7,11,15-tetramethyl-2-hexadecene	1.03	0.44	0.91

Since the components of HTL bio-oil are complex and diverse, the mechanism of HTL process of microalgae has not fully uncovered and explained appropriately to date [15]. However, the bio-oil obtained from hydrothermal liquefaction treatment also needs upgrading before it is suitable for use on engine. The main target of upgrading is to remove oxygen and nitrogen content, reduce the viscosity and

acidity. While the oxygen content is relatively low, approximately 75% to 80% of the nitrogen remains in the bio-oil after the HTL treatment. In order to make the oil applicable for engines, a huge amount of nitrogen content needs to be removed from the crude oil. However, the nitrogen content mostly attaches in the heterocyclic components so it is difficult to remove a huge amount of nitrogen, which is a bottleneck for the HTL method.

1.2.3 COMPARISON OF PYROLYSIS AND HTL CONVERSION

According to previous studies, the hydrothermal liquefaction (HTL) process produces a higher quality bio-oil than pyrolysis when used for microalgal feedstocks. For example, the oxygen content of HTL bio-oil ranges between 10 % to 20 %, while pyrolysis bio-oil can have up to 40% oxygen (figure 5) [16]. Accordingly HTL bio-oil has a higher heating value of around 35 MJ/kg, competitive with conventional fossil fuels whose heating value is between 40 and 45 MJ/kg. On the other hand, the heating value of pyrolysis oil ranges between 16 to 19 MJ/kg, mainly due to the oxygen and water content of the oil [16-18].

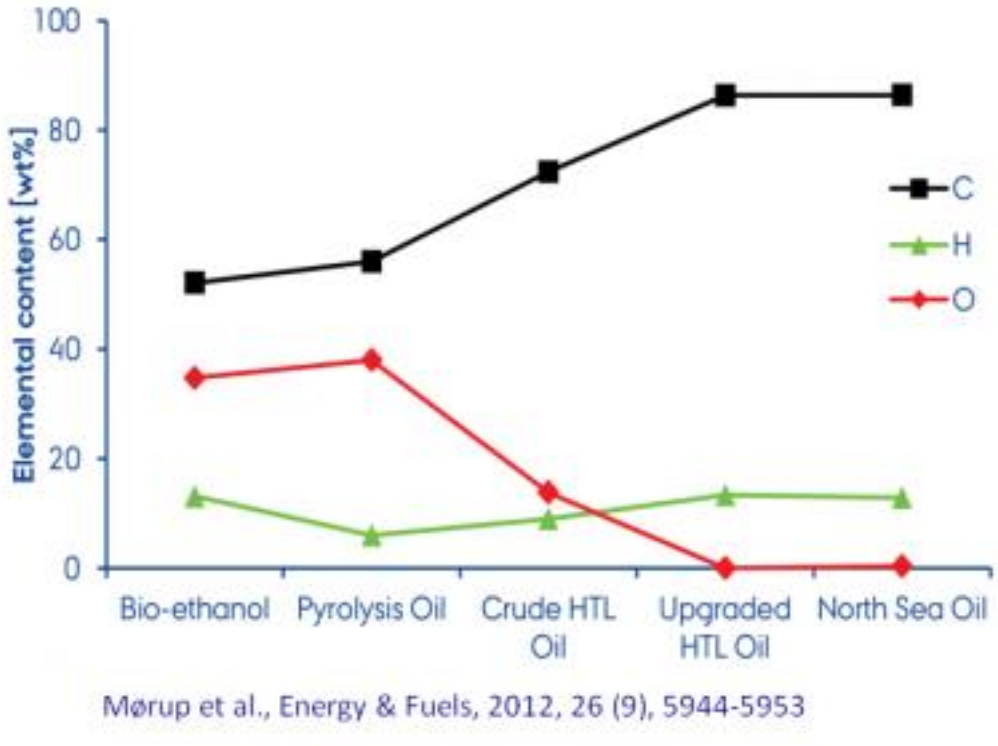

Figure 3 Main elemental composition of different fuels, reproduced from [18].

1.3 UPGRADING OF BIO-OIL

As the hydrothermal liquefaction (HTL) bio-oils cannot be used directly, upgrading of the bio-oil is necessary, which means reducing the acidity, nitrogen and oxygen content to improve stability performance of the fuels [11].

There are two main methods for the upgrading process, namely hydrotreating and hydrocracking. The hydrotreating upgrading process uses high pressures of hydrogen and promotes a range of reactions that eventually reduce the organic compounds in the bio-oil stripping N as ammonia and oxygen as water. The hydrocarbon portion left is suitable for use as a liquid diesel or light combustible gas. Alternatively, hydrocracking is a catalytic cracking process, which is aiming for converting the aromatics and naphthenics into paraffinic components (saturated alkanes) under a relatively high hydrogen pressure. For example, the benzene ring can be turned to hexane via hydrocracking method. Therefore, using porous materials, for example zeolite as catalyst to upgrade the HTL bio-oil is a potential solution in bio-oil refining [12].

The major upgrading process for HTL bio-oil consists of hydrodeoxygenation and denitridation reactions, which reduce the acidity, strip nitrogen and reduce the molecular weight of the heavier components. Under this situation, the heavy components and some of the acids are converted into hydrocarbons, mainly within the C_1 to C_{18}, range though some heavy fractions remain in the liquid oil, and can contain heteroatoms [19].

Due to the high diversity of components in the bio-oil, there are a complex network of catalytic reactions in the upgrading of HTL oils that include cracking, decarbonylation, decarboxylation, hydrocracking, hydrodeoxygenation, hydrogenation and polymerization [20-22]. Examples of the possible catalytic reactions in bio-oil upgrading are given in figure 4 below. The most relevant mechanism to bio-oil upgrading is probably hydrodeoxygenation (HDO) which is normally carried out at a range of temperature between 250 and 450 °C[23, 24].

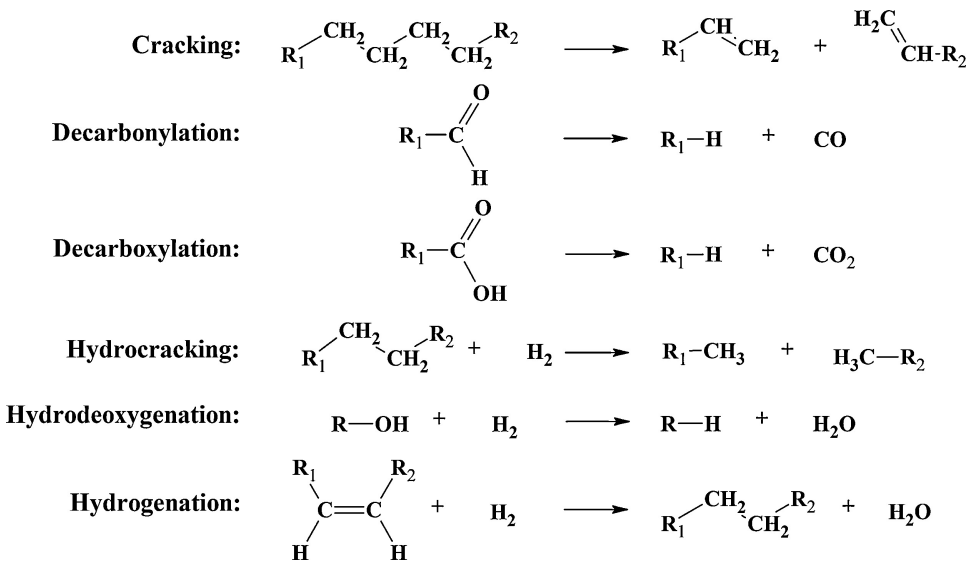

Figure 4 Examples of catalytic reactions in upgrading bio-oil, adapted from [22].

Hydrogen consumption is also a critical factor in the economic upgrading of HTL oils. The relationship between hydrogen consumption and degree of deoxygenation is given in figure 7. In this graph, the X-axis represents the degree of deoxygenation, the Y axis means the H_2 consumption in mol/kg. There are two lines, one is bold line another is dotted line in the graph, which indicate measured and theoretical hydrogen consumption respectively. The degree of deoxygenation increases sharply with the hydrogen consumption [24]. While the degree of deoxygenation roughly follows the stoichiometric requirement below 80% deoxygenation, a large amount if needed to fully deoxygante the oil. This is presumably due to the highly reactive oxygenates being easily converted into hydrocarbons with quite low hydrogen consumption, these include species such as acids, alcohols and ketones. However, there are oxygen that bound in the more stable compounds, so the more complex molecules are required more hydrogen at the beginning, which cause the hydrogen consumption is more than stoichiometric prediction [23].

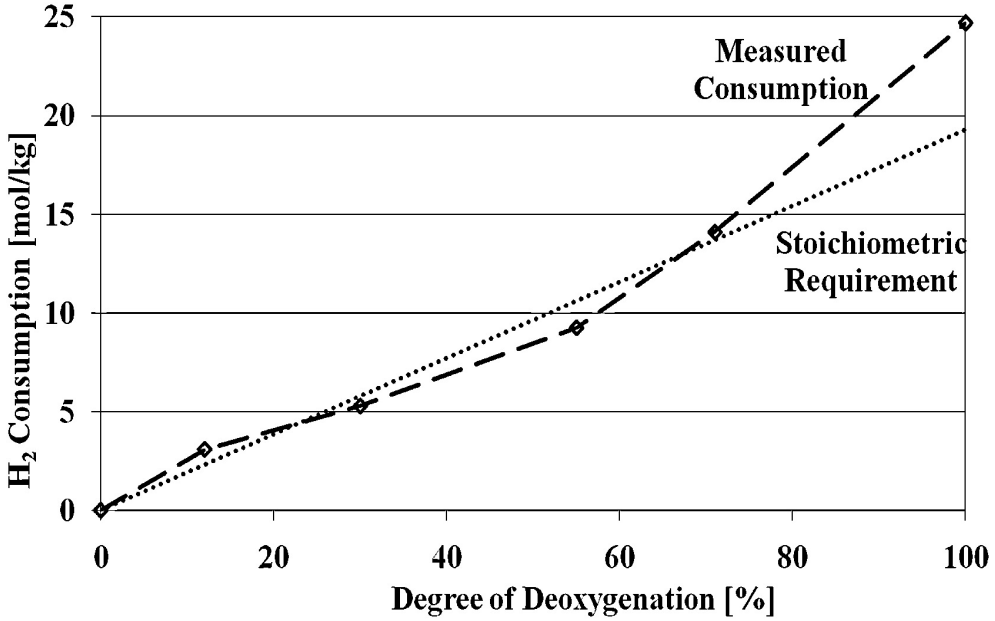

Figure 5 The relationship between the degree of deoxygenation and hydrogen consumption to indicate the exceed hydrogen consumption. Taken from [22].

The hydrotreating process requires extra hydrogen input to enable and maintain the whole reaction process [11], which causes an extra energy consumption since it requires extra hydrogen gas and high pressure usually above 40 bar. Alternatively, some research has been conducted in to using hydrogen donors such as formic acid in the reaction, formic acid has a relatively low cost and can decrease the reaction pressure to some degree. Moreover, using hydrogen donors for bio-oil upgrading can save the hydrogen, since it does not need additional hydrogen input during the reaction. Under this situation, a high reduction of oxygen content in the model oil from 41.4 to 2.8 wt% is also achieved. [25]

According to the information above, the hydrogen is used for two main aspects, which are removing oxygen and saturating double bonds, to get the decrease of O/C ratio and the increase of H/C. Therefore, the results cause the heating value of bio-oil increasing, which improves the grade of bio-oil [26].

Since the high diversity components in the bio-oil, and the wide range of catalytic reactions, it is difficult to specify which reactions a promoted by which catalyst of to determine the optimal catalyst for the upgrading. For the oil, the hydrodeoxygenation, hydrogenation and depolymerization as well as addition reactions of the smaller components are the most sought after reactions. This promotes the removal of oxygen and nitrogen reduces the corrosivity which is vital in a transportation fuel.

1.3.1 ENERGY CONSUMPTION

Although bio-oil gained from hydrothermal liquefaction (HTL) process has the lower oxygen content level compared to pyrolysis bio-oil, the bio-oil upgrading process of HTL bio-oil still requires a relatively high reaction temperature. Temperatures between 250 °C – 450 °C are common, depending on the system and catalyst used [27, 28]. These are demanding conditions and can severely reduce the energy return on investment.

To this end, there are several options to reduce the temperature during the upgrading process. The first option is stabilizing the bio-oil before the upgrading process. Using a relatively lower temperature to stabilize the bio-oil first, the reaction temperature for the bio-oil upgrading process can be decreased to a range of 200 to 300 °C [29]. The purpose for this method is removing oxygenates in the bio-oil partly, which can make the bio-oil more stable compared to the non-stabilized bio-oil. In this situation, the coke formation rate is decreased to some degree, resulting in the reaction temperature going down [28].

Hydrogen consumption is one of the main restrictions of the bio-oil upgrading process becoming applicable to the petro-chemical industries, and also hinders bio-oil becoming a complete replacement of conventional fossil fuels [30]. To reduce the hydrogen consumption in bio-oil upgrading process, there are several aspects can be optimized during the upgrading reactions. The first aspect can cut down the hydrogen consumption is stabilizing the bio-oil before or during the upgrading process. For example, conducting the thermal chemical conversion during the process producing bio-oil is a solution to decrease the hydrogen consumption [31]. Another option is using mixture of conventional oil and bio-oil, which also can reduce the hydrogen consumption during upgrading process [32, 33].

Alternatively, the hydrogen consumption can be reduced by introducing reactants with hydrogen content, such as ethanol, formic acid and acetic acid. With these chemicals hydrogen can be produced and released during the upgrading process because of the high reaction pressure and temperature [10, 25]. For example, formic acid can be effectively used at 300 °C and the pressure can also maintain in a low level of 2 to 12 MPa [25]. Under this situation, it can be easily seen that the energy consumption not only just for temperature reduction, but also for pressure reduction during the bio-oil upgrading

process, which improve the reaction energy consumption in both aspects. Though this saving might not compensate for the cost of formic acid.

Finally, to cut down the hydrogen consumption by optimizing the elemental reactions and catalyst in the upgrading process seems the most sensible option [30]. This can be achieved by applying the metal load or mesopores catalyst in the reactions. Loading the Pt or Ru on the catalysts to use in the bio-oil upgrading process can reduce the temperature to 250 °C, since the metal loading catalyst can decrease the coke formation rate and diffusion limitation [28]. For this reason, the reaction can take place under a much lower temperatures.

1.3.2 CATALYSTS FOR UPGRADING

As the upgrading procedure is very important to the bio-oil, catalysts using in the upgrading process have been extensively studied. Catalysts have been applied in the bio-oil upgrading mostly are Ni or Co with Mo as metal catalyst, noble metals, such as Pt, are also applied in the upgrading for increasing the capacity of catalysts. Another type of catalyst is widely use is activated carbon. However, the high cost, fast deactivation and poor particle selectivity are restrictions for all these catalysts to be ideal catalyst in the bio-oil upgrading [30,45,46,47].

An alternative more inexpensive catalyst system is zeolites. With their porous structure, zeolites have been widely applied in the wider petrochemical industry as well as in in refining process of bio-oil products [34]. The unique structure of zeolite provides a high surface area, and gives a high performance in shape selectivity, which is a necessary factor in bio-oil upgrading because of the diversity in the components.

There are a number of elementary parameters that can affect the performance of a zeolite catalyst. First of all, large pore size will offer more accesses to reactants compared with smaller pore size. Secondly, acid sites also affect the upgrading reaction, which presents in the accessibility of reactants increase with grow of acid sites; acid sites' increase can be achieved through alkali-treatment. Another factor cannot be ignored is ratio of Si/Al, decrease of Si/Al ratio leads an increase of acidity of zeolite, which improves the conversion of reactants [35].

In order to reduce the oxygen and nitrogen content amount in the bio-oil to make it feasible for the engine usage, zeolite is mostly applied as catalyst in the upgrading process under a high temperature. For example, a variety of zeolite were tested in the hydrodeoxygenation reaction, the H/C ratio was increasing from 0.9-1.5 to 1.3-2.0. While the O/C ratio was decreasing from 0.3-0.5 to <0.1 [22].

In spite of the advantages of using zeolite as catalyst in bio-oil upgrading, zeolite also introduces a disadvantage that known as the low access rate of molecules during the upgrading process [36]. Another issue that may occur during the catalytic reaction is adsorption effects of unwanted reactants or products. This negative effect can cause steric constraints on zeolite, which can decline the available volume of zeolite crystals that is a main barrier in zeolite catalytic reactions [37].

Although zeolites have been extensively studied in the bio-oil upgrading, the upgrading of HTL bio-oils has not been studied using zeolites as catalysts. HTL oil has a relatively high nitrogen content and they are mostly attach to the heterocyclic compounds, so the high particle selectivity of zeolite could potentially be a good solution to removing nitrogen content from the oil.

As the zeolite-Y (FAU), modernite (MOR) and ZSM-5 (MFI) are three main types are used in the upgrading of bio-oil, they are also introduced to this project as upgrading catalyst to study their properties and performance.

1.3.2.1 SUITABLE ZEOLITE CATALYSTS

Zeolite-Y (FAU)

Zeolite Y (FAU), consists of sodalite cages connected through D6R units. The large pore, also called the alpha-cage, is formed by a 6-, 8- and 12-membered rings, and has a relatively large aperture diameter of 7.4 Angstroms (Å). The inner cavity has a diameter of 12 Å and is surrounded by 10 sodalite cages [38]. There is a 3 dimensional diagram of zeolite Y crystal structure, showed in the figure 6 (taken from the international zeolite association)[39].

Zeolite Y is used commonly as acidic support catalyst in hydrocracking

process in petro chemical industry because of its good catalytic capability.[38] The reason why zeolite Y has a good performance on catalytic hydrocracking is that it contains a large number of Brønsted acid sites, which are also known as active sites for the reactions. With a relatively large pore size; zeolite Y can also give an easier access for heavy components in bio-oil compared to other structures. To achieve a higher effect in upgrading, the zeolite Y can be dealuminated to increase its acidity, which can improve the catalytic capability in the hydrocracking reactions [40].

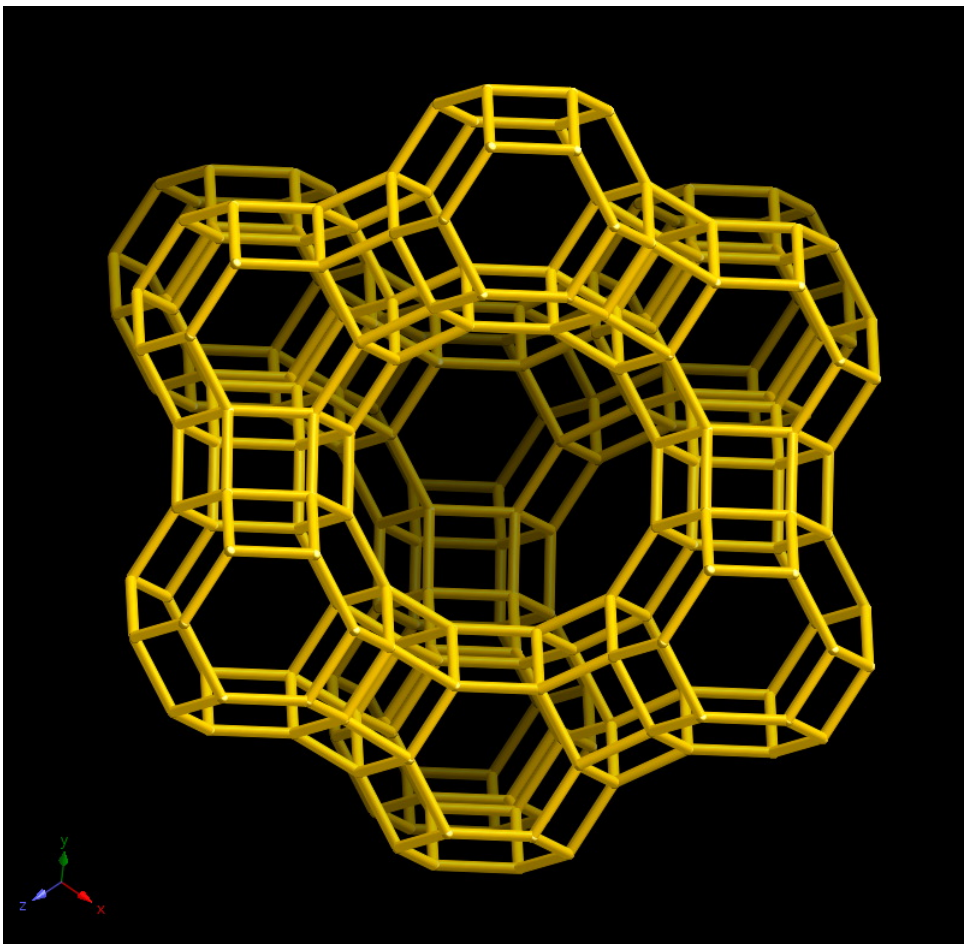

Figure 6 Structure of FAU framework, which is part of zeolite-Y. Taken from international zeolite association website. [39]

MORDENITE (MOR)

In the crystal structure of mordenite, the four-membered, six-membered and eight-membered rings are commonly seen. However, there is also an abundance of five-membered rings. Two parallel five-membered rings sharing two tetrahedron form the

characteristic *mor* building unit observed throughout the structure. The five-membered rings can be further interconnected, so they can form eight-membered rings, twelve-membered rings and so on. 12-MR is oval shaped, the maximum and minimum diameters being 0.7nm and 0.58nm respectively, (averaging 0.66nm). Therefore, the crystal form of mordenite contains straight-shaped pores, the largest channel being formed from the twelve-membered rings. The channels are oval-shaped, with a major axis diameter of 0.695nm and a minor diameter of 0.581nm,. Between the main channels of mordenite there are small pores interconnected with each other, but since these pore apertures (about 0.39nm) are very small, only the main channel is accessible to most molecules [41]. Figure 7 shows the three dimensional crystal structure of mordenite (MOR)[42]:

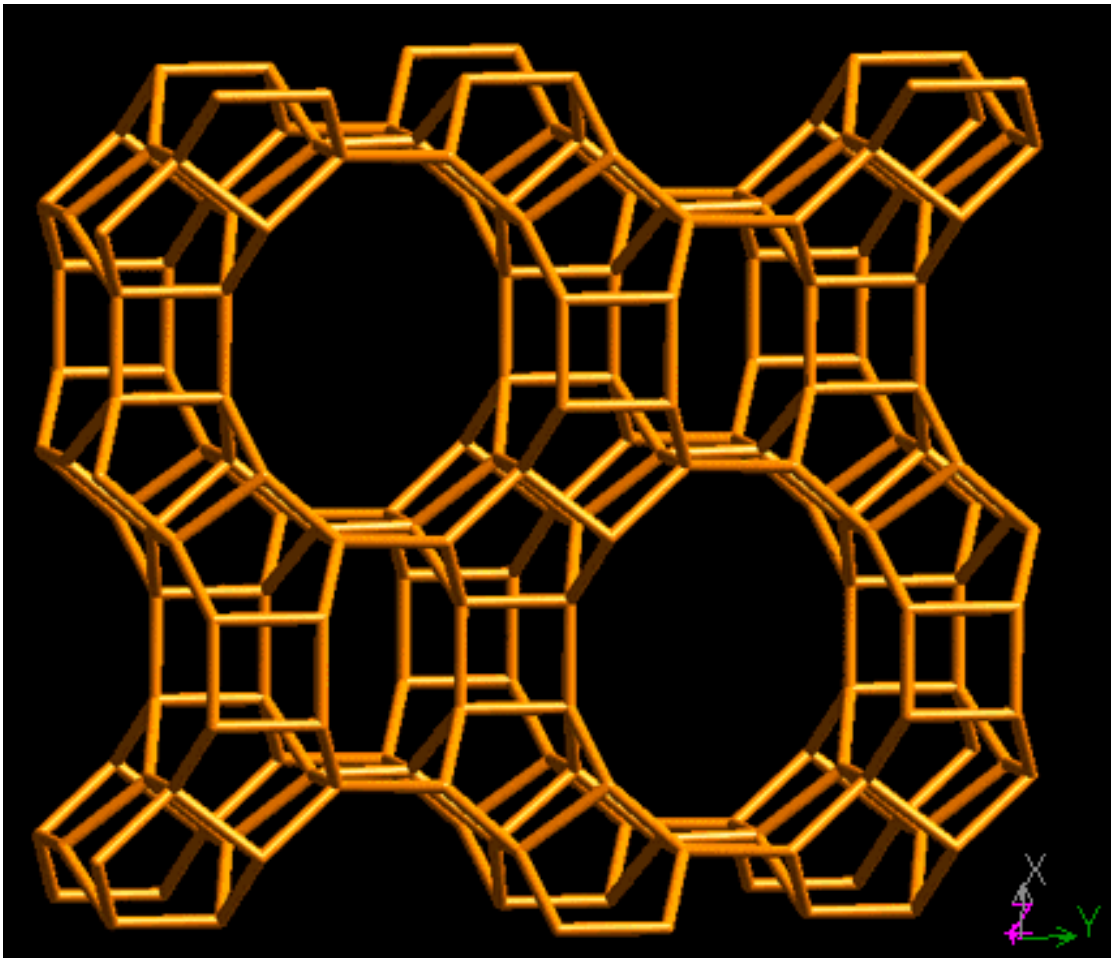

Figure 7 Structure of mordenite (MOR) framework. Taken from international zeolite association website. [42]

Like faujasite, mordenite is also widely applied in the petro chemical industry. Synthetic Mordenite is used as a catalyst in the petrochemical industry for the acid-catalyzed isomerization of alkanes and aromatics. This is due to the narrow 12-MR channels. However, in

comparison to zeolite Y (FAU), mordenite has a lower activity in catalytic reactions due to its smaller pore size. To improve the performance of mordenite in catalytic reactions it is commonly treated under dealumination. Dealumination of zeolites is removal of aluminum from the framework, which can increase the amount of active sites to improve the catalytic capability. Dealumination also creates a secondary mesoporous structure, which results in an improvement of catalytic activity and shape selectivity.[43, 44]

ZSM-5 (MFI)

Zeolite ZSM-5 contains ten-membered rings, however the basic structural unit is composed of eight five-membered rings. It has no special structure A, X, or Y-type zeolite cage, as its channel is its cavity. The framework consists of two intersecting cell system components, the straight-shaped channel is oval-shaped, the major axis diameter being 5.7 ~ 5.8 Å and the minor axis 5.1 ~ 5.2 Å. The other component is the "Z" shaped transverse channels, with a near circular cross section and a diameter of 5.4 ± 0.2Å ZSM-5 is classed as a medium pore zeolite[45]and has an MFI-type framework which is shown in figure 8 [46].

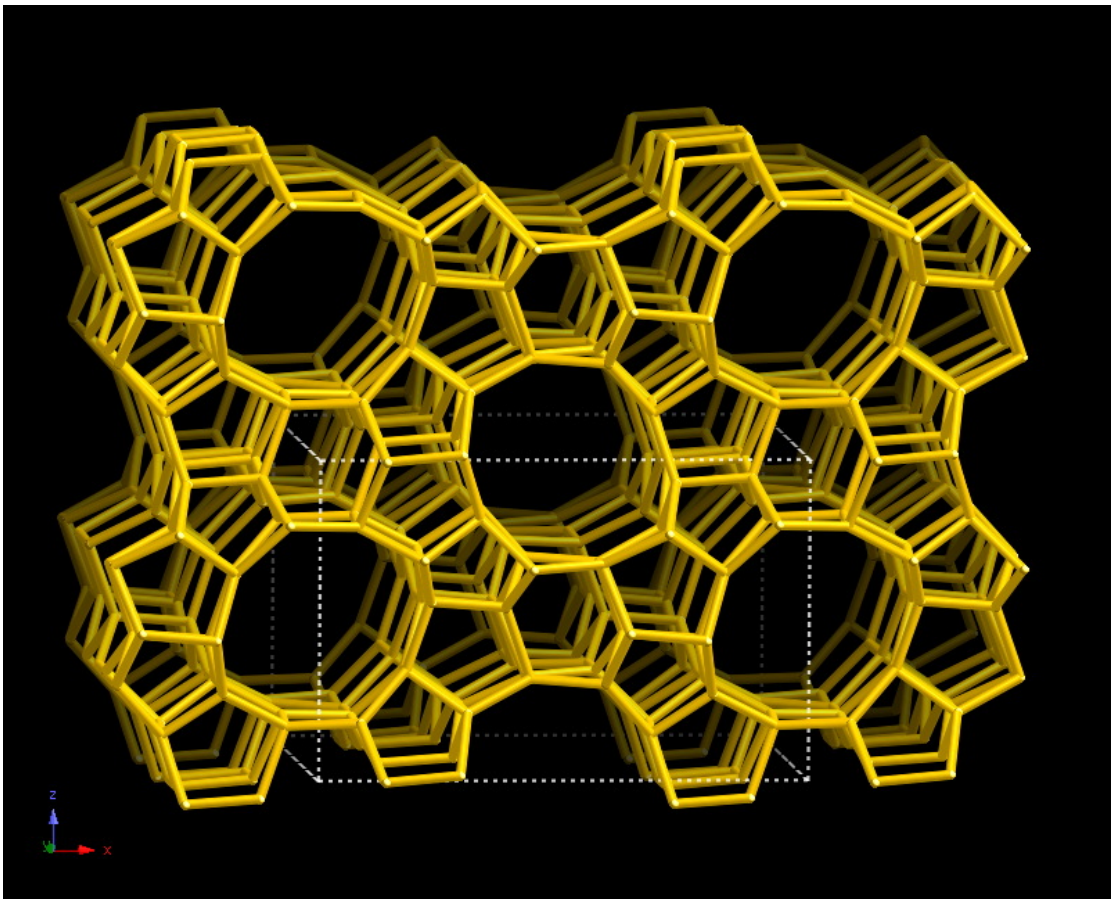

Figure 8 Structure of MFI (ZSM-5) framework. Taken from international zeolite association website. [46]

As ZSM-5 has a high surface area, active sites and shape selectivity, it shows a good performance as a catalyst in reducing the oxygen content in aromatics by catalytic reactions in petro chemical industries.[47] However, there are a number of issues in using ZSM-5 as a conventional zeolite catalyst in bio-oil upgrading. For example, fast deactivation of the catalysts by coke deposition, low organic liquid yield and the formation of polycyclic aromatic hydrocarbons have all been observed [48]. There is no need for ZSM-5 to dealuminate, since ZSM-5 already has a relatively high Si/Al ratio, and dealuminating methods will not offer an improvement for its catalytic capability. Therefore, a high Si/Al ratio ZSM-5 is the most suitable catalyst for bio-oil upgrading.

1.3.2.2 MODIFICATION OF ZEOLITES

In order to improve the performance of zeolites in catalytic reactions, especially in petrochemical industries, zeolites with hierarchical structures can overcome the drawbacks of conventional zeolites.

Hierarchical zeolites refer to zeolite structures containing both micro-pores and mesopores in one zeolite structure. By adding mesoporous structure to classical microporous zeolites, diffusion limitations of classical zeolites, which prevent big molecules getting access to the active sites, can be overcome. In this way, hierarchical zeolites can offer more accessibility of large molecules than conventional microporous zeolites. At the same time, it also can maintain the advantages from micropores such as high acidity, and stability [49].

There are a large number of methods to synthesize hierarchical zeolites. The most commonly used methods are explained as follows: (1) desilication [50]; (2) dealumination[51]; (3) solid templating[52]; (4) pillaring and delamination[53]. In this project, to improve the catalytic capability, the dealumination method has been used.

Another method to improve zeolite catalytic performance is ion exchange with transition metals, which involves loading metal ions onto zeolite particles. To this way, the zeolite gains a higher selectivity and activity in reactions, especially in adsorption and decomposition reactions. The most commonly used metals are Fe, Cu, Co, Mo, and Pd. For some specific zeolites, for instance, zeolite Y (FAU), loading with metal ions can also enlarge the surface area, which can also improve the catalytic activity.[49, 54]

1.3.3 CATALYST CHARACTERIZATION

Zeolites, with their complex framework and variable pore size, need to be characterized properly via several methods to confirm the unit cell parameters, correct framework and silicon to aluminum ratio.

The following methods were used for sample characterization:

1.3.3.1 POWDER X-RAY DIFFRACTION

X-ray diffraction is a routine method for determination of sample purity and crystal structure analysis. Powder X-ray diffraction is more frequently used for characterizing zeolites compared to single crystal X-ray diffraction, owing to the microcrystalline particles resulting from common synthesis methods.

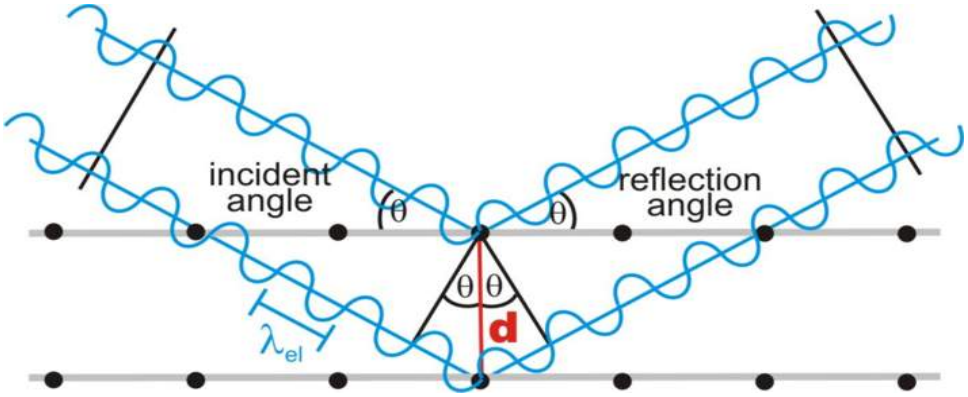

Figure 9 Bragg's law of diffraction. Reproduced from [54].

Zeolite crystals are represented as regular arrays of atoms, which means the single unit structure of zeolite is repeatable. The unit structure also called unit cell, which represents the smallest repeatable structure in zeolite crystals. Therefore, the regular array will produce a regular array of X-ray waves when the X-ray beam strikes the crystals. The position of the reflections is determined by Bragg's law (1)[55]:

$$2d \sin\theta = n\lambda \tag{1}$$

Here, d is the spacing between diffracting planes, θ is the incident angle, n is any integer and λ is the wavelength of the X-ray beam.

Based on the powder X-ray diffraction data, the crystal properties can be also estimated. From the peak positions, the peaks can be indexed to calculate the unit cell parameters. Moreover, the peak shapes give a rough indication of crystal size[56]. The crystal size can be calculated by the Scherrer equation (2):

$$L = {K\lambda}/{\beta_{(hkl)} \cos\theta} \tag{2}$$

Where:
$L =$ Crystal size
$K =$ Scherrer constant = 0.89
$\lambda =$ Wavelength of the X-ray
$\beta_{(hkl)} =$ Full width at half maximum for the major peak of the X-ray diffraction
$\theta =$ Bragg angle of the incident X-ray

1.3.3.2 SOLID STATE NMR

Solid-state nuclear magnetic resonance, also known as SS-NMR, is an analytical technique for detecting the local environment of elements in solid state materials. This technique is often used as a complementary method to X-ray diffraction to determine the structure of zeolites.

NMR spins by magnetic or electric fields interact to excite the nuclei. Bonding between atoms can produce interaction between nuclei. In general, these interactions are dependent on orientation. In solid-state NMR in two directions dependent interactions are common chemical shift anisotropy (CSA) and the dipolar coupling between nuclei. There are many more such interactions, such as nuclear magnetic resonance anisotropy J- coupling, or in related fields, such as the g tensors in electron spin resonance [57].

After the split of energy level, high energy level and low energy level in the number of nuclear distribution change, and in line with the principle of Boltzmann distribution: the number of nucleons in a low energy level and a smaller number of more high energy level, and ultimately produce a vertical direction net magnetization vector straight on. This magnetization vector in the oscillating radio frequency magnetic field being along the x-y plane will eventually produce a torque in the vertical direction of the magnetization vector is rotated a specific angle. Magnetization vector during the recovery process, the interaction in solution NMR mainly include: chemical shift relatively weak interaction, J- coupling, etc., and between relatively strong molecular dipole spin coupling interaction in most systems due to thermal motion of molecules is averaged. However, solid-state NMR experiments in solid state due to molecular making it difficult to make the system of the dipolar spin coupling effects through the thermal motion of molecules and averaged.[58, 59]

According to the results of SS-NMR, the T-O-T angles can be calculated as a method to determine whether the structure of zeolite is squeezed after ion exchange. The peak positions in NMR are a function of the T-O-T angles in zeolite framework has already been proved. Si NMR chemical shifts are related to the value of four Si-O-T bond angels (α) averagely. The equation is as followed[60]:

$$\delta\, Si\ (ppm) = -5.230 - 0.570\ (\alpha) \qquad (3)$$

Based on NMR spectrum, the Si/Al ratio can be also obtained. The

equation for Si/Al ratio is shown below:

$$\frac{Si}{Al} = \sum_{n=0}^{n=4} I_{Si\ (nAl)} \Big/ \sum_{n=0}^{n=4} \left(\frac{n}{4}\right) I_{Si\ (nAl)} \qquad (4)$$

Here, I is the intensity of peaks; n is the number of aluminum atoms coordinated to each SiO_4 tetrahedron through bridging oxygen atoms[61].

1.3.3.3 SCANNING ELECTRON MICROSCOPY

Scanning electron microscopy (SEM) is for studying the crystal morphology of zeolite crystals. Scanning electron microscopy is based on the interaction of electrons with matter. SEM is the use of a very fine focus high-energy electron beam on the sample in scanning mode. This results in a variety of physical information including sample surface morphology.

When high-energy electrons are incident on the sample surface, electron bombardment causes excitement of the sample, to generate secondary electrons, Auger electrons, characteristic X-rays and X-ray spectra and backscattered electrons.. At the same time it can produce electron - hole pairs lattice vibrations (phonons) and electronic oscillations (plasma)[62]. To observe the shape and size of the zeolites, low accelerating voltages (5-10 kV) are used.

1.3.3.4 ENERGY DISPERSIVE X-RAY SPECTROMETRY

Energy dispersive X-ray spectrometry, also known as EDX, is a commonly used method for elemental analysis of materials. It relies on the interaction of electron beam with the samples. It's largely due to the principle that each element has a unique atomic structure, which produces allows a unique set of emission peaks in its X-ray spectrum. A high-energy beam charged with electrons or protons, or a beam of X-rays is focused on the sample to stimulate the emission of characteristic X-rays from sample.[63]

However, EDX is affected by several factors that can make a difference to results. Measuring samples require samples to be attached onto the holder with carbon tape, which will create a carbon peak in the results; even if the sample does not have any carbon originally. Another issue

is that the results rely heavily on the point that is sampled, which can cause large differences between samples some times. Therefore, EDX can only be a complementary tool for quantitative elemental characterization.

1.3.3.5 FT-IR

FTIR is Fourier transform infrared spectrum analysis (Fourier Transform infrared spectroscopy). FTIR is the use of infrared spectroscopy using a Fourier transform spectrometer, consisting of a light source (silicon carbide, high-pressure mercury lamp), Michelson interferometer, detector and interferometer components. The central part of the Fourier transform infrared spectrometer is a front Michelson interferometer. The sample is placed in the detector, and scanned though different frequencies of infrared light. The detector receives the interference light intensity changes, resulting in a sample interferogram. This interference pattern is, obtained by means of Fourier transform function of light intensity varied in the frequency domain. The main structure of FT-IR shown in figure 10.

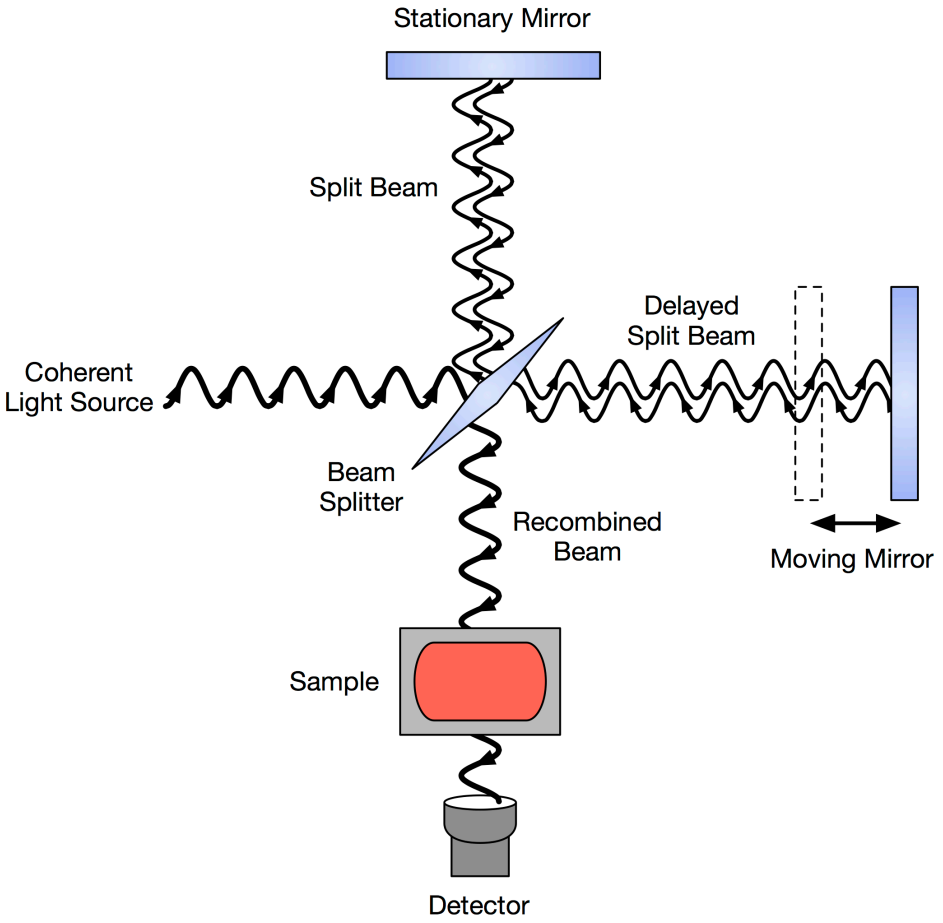

Figure 10 Schematic diagram of the core part of Michelson interferometer FT-IR. Taken from Internet resource.

Optical light is passed through a beam splitter (e.g. a half mirror) splitting into two beams. The two beams are reflected by a fixed mirror and movable mirror back to the beam splitter, a movable mirror at a constant speed in a straight line, so that the two beams by a beam splitter splitting light after the optical path difference is generated interference. After the beam passes through the sample cell, the beam containing sample information reaches the detector, then the Fourier transform of the signal is processed. The final transmittance or absorbance is obtained as a function of wavenumber or wavelength of the infrared absorption spectrum.[64]

1.3.3.6 BET specific surface area

Specific surface area refers to the area of total surface area of all particles in per gram of the material. It is an essential parameter for the material using as catalyst in the reactions to determine its capability of catalysis. BET is a short name for a theory that presented

by Stephen Brunauer, Paul Hugh Emmett and Edward Teller in 1938. It explains the theory of gas molecules on a solid surface adsorption phenomenon.[65]

The BET theory is an important theoretical basis solid surface analysis and research. Its principle is to find different partial pressures of the absolute amount of sample to be tested for nitrogen adsorption by BET theory to calculate the monolayer adsorption capacity, thereby obtaining the specific surface area.[65]

1.4 SUMMARY

With the growing demand for transportation fuels, and an increasing awareness of the environmental damage that conventional fossil fuels cause, advanced biofuels are being developed and studied. First-generation and second-generation biofuels, which are using food crops and cellulose as feedstocks respectively, cannot meet the energy requirements of large-scale industrial and civil applications currently, since the product yield of using food crops and cellulose are relatively low. This can cause a series of problems, for instance, shortage of arable land. Third-generation biofuels that use microalgae as a feedstock is regarded as one of the most promising solutions to overcome the global energy crisis since the yield of micro algal bio-oil is relatively high compared to the former generation of biofuels. Moreover, microalgae is easy to grow in the contaminated water and does not occupy arable land.

Thermochemical conversion is regarded as the main pathway to generate the bio-oil from the microalgae, which includes the pyrolysis and hydrothermal liquefaction process. Compared with pyrolysis bio-oil, bio-oil obtained via hydrothermal liquefaction has a higher hydrogen content and a lower oxygen content. It is also unnecessary to dry the algae prior to conversion, therefore, hydrothermal liquefaction is a promising pathway to producing bio-oil with microalgae feedstock.

As the bio-oil gained from microalgae cannot be employed in engines directly, an upgrading process for bio-oil is necessary. Zeolites are one of the most commonly used catalysts in conventional upgrading processes as well as upgrading of pyrolysis oils, because of its microporous structure. However, the conventional zeolite catalyst is restricted by diffusion limitations and rapid deactivation in the bio-oil upgrading process. Moreover, the diversity of reactions in bio-oil

upgrading also limits the performance of the catalyst.

To this end, optimizing the zeolite catalyst is becoming an issue that needs to be solved. For optimizing the zeolite catalyst, there are two main approaches: introducing hierarchical structure and ion exchange. Hierarchically structure zeolites, which mean the structures contains both micropores and mesopores or macropores, is favorable for bio-oil upgrading since it can solve the diffusion limitation and improve the accessibility of the large molecules. When it comes to ion exchange, exchanging the ions in a zeolite structure can change the Si/Al ratio, which can result in an increase of active sites. Under this situation, exchanged zeolites can be much more effective than non-ion exchanged zeolites, and can lead better performance in bio-oil upgrading process.

2 AIMS

The aim of this project is to synthesize and well characterize a range of zeolite catalysts and test their hydrogenation performance on a model HTL bio-oil, including the hydrogenation of heterocyclic and alkyl amines, key components in algal HTL bio-oils. The key objectives are

- Synthesis of FAU, MOR and ZSM-5 zeolite catalysts with alternative counter-ions.
- Characterize the zeolites with XRD, EDX ,SEM, SS-NMR, BET and FT-IR methods to confirm their framework and determine other relevant parameters
- Screen the catalysts for their performance in hydrogenating a model oil, created to mimic algal HTL bio-oil.

3 EXPERIMENTAL

In this project, the experimental section is divided into two main parts. The first section describes the synthesis of three types of zeolite: FAU, MOR and ZSM-5 in original sodium form, then exchanging sodium cations with the ammonia and hydrogen ions. The second stage is conducting conversion tests with the model oil using the zeolite samples as catalyst.

3.1 SYNTHESIS OF ZEOLITES

Zeolite-Y, mordenite and ZSM-5 are quite different types of zeolite; their crystal structures, size and shape also vary. Therefore, their synthesis conditions and methods are different in many respects. However the synthesis procedures still consist of two steps: seeding gel and feedstock gel.

3.1.1 ZEOLITE-Y (FAU) SYNTHESIS

FAU-type zeolites can be synthesized in different conditions with different types and batch compositions. Since its stability and micro-porous structure, the Linde Type Y FAU is selected as catalyst with an overall batch composition of 4.62 Na_2O : Al_2O_3 : 10SiO_2 : 180H_2O[66].

To obtain 10.7 g product, the seeding gel was made by 6.65 g water, 1.36 g sodium hydroxide and 0.7 g sodium aluminate, stirred in a 50 mL plastic bottle until dissolved. The next step was adding 7.57 g sodium silicate solution, and stirred moderately for at least 10 minutes. The bottle was sealed and the seeding gel left at room temperature for 1 day.[66]

For the feedstock gel, 0.05 g sodium hydroxide and 4.36 g sodium aluminate in 43.66 g deionized water was stirred in a plastic bottle until dissolved. After that, 47.48 g sodium silicate solution was added to the mixture, stirred vigorously with a high-shear turbine mixer until the gel appeared relatively smooth. The bottle was sealed until the seeding gel was ready to be added.[66]

Finally, the 5.5 g seed gel was slowly added to the feedstock gel under high shear stirring. The bottle was moved during the mixing process

to ensure the entire gel was mixed equally with the high shear stirrer for at least 20 minutes until the whole phase appeared smooth and well-proportioned as a white thick solution.[66]

The last step was crystallization. The mixed gel was transferred to a tightly sealed polypropylene bottle and put into the oven at 100°C for 6 hours. After heating, the solution appeared as a white precipitate with clear solution above. The sample was then separated by vacuum filtration and washed until the filtrate was of neutral pH. The powder was then dried in an oven at 100°C over night to make the sample ready to run the XRD process.

3.1.2 MORDENITE SYNTHESIS

Mordenite is selected as one of the catalysts because of its low aluminate proportion and mesoporous structure. Its batch composition is 6 Na_2O : Al_2O_3 : 30 SiO_2 : 780H_2O[67].

To synthesize mordenite crystals, it does not require an initial seeding step. 1.15 g sodium hydroxide was dissolved in 40 g deionized water, and then 0.52 g sodium aluminate was added with stirring until the solution became clear. 9.7 mL Ludox (HS-30) was added to the solution, and the solution stirred for 24 hours.[67]

After stirring, the solution was transferred into stainless steel autoclave with a Teflon liner. The autoclave was heated in an oven to 190℃ for 3 days. Once the autoclave had cooled to room temperature, the sample was separated by vacuum filtration and washed until the filtrate was a neutral pH. The powder was then dried in the oven at 100°C for 24 hours.[67]

3.1.3 ZSM-5 SYNTHESIS

ZSM-5 is a conventional catalyst applied in the bio-oil upgrading process, which it has been studied widely. High-alumina ZSM-5 (MFI) was selected in this project to test its ability for bio-oil upgrading. Although, the material is named high-alumina ZSM-5, the proportion of aluminum is actually quite low, being only 7 percent in overall silicon and aluminum. The batch composition of the high-alumina ZSM-5 is 3.25 Na_2O : Al_2O_3 : 30 SiO_2 : 958 H_2O (exclusive of seeding gel)[68].

To synthesize ZSM-5 crystals, an organic structure directing agent (OSDA) was used in the synthesis process. First, to make the seeding gel 0.69 g sodium hydroxide and 1.17 g tetrapropylammonium hydroxide (TPA-OH) were added to 35.515 g distilled water, and stirred thoroughly until dissolved. 7.945 g silicic acid was added slowly in portions under stirring. the resulting mixture was shaken for one hour at ambient temperature then put into the oven at 100℃ for 16 hours.[68]

For the feedstock gel, 0.458 g sodium hydroxide and 0.52 g sodium aluminate was added to 43 g distilled water, dissolved and mixed thoroughly. 5.635 g silicic acid was added to the mixture in portions under stirring, and then stirred vigorously for at least one hour under ambient temperature. 2.565 g of the seeding gel was added to the feedstock gel and the mixture was stirred for one hour.[68]

The mixed gel was transferred to a Teflon liner, and sealed in a stainless steel autoclave. The autoclave was put into the oven at 180℃ for 40 hours. After the crystallization, the autoclave was cooled down at room temperature before opening. The crystals were then separated by vacuum filtration and washed until the filtrate was neutral pH. The sample was then dried in the oven at 100℃ for 24 hours.[68]

The synthesis of ZSM-5 introduces the use of TPA-OH as template. The TPA-OH has to be removed from the zeolite's pores before the sample can be applied in the experiment. To remove the template, the tube furnace was used to calcine the sample and remove the TPA-OH completely without breaking the structure of ZSM-5. The tube furnace was evacuated before heating the sample in the tube. A vacuum pump was connected to the tube to remove the air and to extract the water and gas phases during the heating process. After evacuation, the tube furnace was set up with a heating program, which gave the sample a moderate increase and decrease of temperature and did not break the structure of the sample during the ramping process. The furnace-heating program is shown below:

$$RT \xrightarrow{75\ mins} 100℃ \xrightarrow{100\ mins} 200℃ \xrightarrow{200\ mins} 400℃ \xrightarrow{200\ mins} 200℃$$

$$\xrightarrow{100\ mins} 100℃ \xrightarrow{75\ mins} RT$$

Here, RT represents room temperature and the stationary duration at each temperature was 2 hours.

The total process took 26 hours to remove the TPA-OH template completely. After calcination, the sample structure was tested by XRD.

3.2 ION EXCHANGE OF ZEOLITES

In order to optimize the ability of the bio-oil upgrading, ion exchange was conducted to increase the number of active sites in the zeolite samples. Under this circumstance, the zeolite will have more acid sites to react with the bio-oil and remove the oxygen and nitrogen components. However, due to ZSM-5 already having relatively low aluminum content, the ion exchange was only conducted on zeolite-Y and mordenite.

3.2.1 ION EXCHANGE OF ZEOLITE-Y

Having a high aluminum content, zeolite-Y needed to be well dealuminated for increasing its active sites, to enhance its ability in bio-oil upgrading.

To this end, 5 g of the original sodium zeolite-Y was mixed with 4 g ammonium nitrite in 60 mL distilled water and stirred for 24 hours. After that, the sample was vacuum filtrated and washed with water until the pH was under 8. The sample was then dried at 100℃ overnight. XRD was used to ensure the structure of the sample did not break or change severely.[69]

The exchanged sample underwent the process a second time, using 6g of ammonium nitrate instead of 4g. Once the sample had been washed and dried it was analysed by XRD again to check the structure was undamaged. After the second ion exchange most of the sodium cations in the zeolite framework will have been replaced by ammonia.

To achieve a high performance on bio-oil upgrading, the ammonia needs to be removed from the sample, to produce hydrogen associated zeolite-Y. In order to remove the ammonia in the zeolite sample, calcination with tube furnace was conducted. The ammonia base zeolite-Y sample is put into the tube and the whole system was evacuated. The calcination program was set up as given previously

After this process, the ammonia base zeolite-Y was converted into the hydrogen base zeolite-Y. The sample was analysed by XRD to ensure the FAU structure was unchanged.

3.2.2 ION EXCHANGE OF MORDENITE

The mordenite sample had a lower aluminum content than zeolite-Y, so less ammonia nitrite was needed for the ion exchange. However, to ensure the sodium base was completely converted, the process was done twice as with the FAU sample.

Primarily, 5 g of original sodium base MOR was added to 1.5 g ammonium nitrite in 60 mL distilled water and stirred for 24 hours. The sample was dried at 100℃ overnight, the MOR crystals needed to be washed with distilled water until the pH was below 8. XRD was used to check the structure of the MOR crystal was complete.[69]

The second round of ion exchange used 2.25 g ammonium nitrite with the sample and was stirred in 60 mL distilled water for 24 hours. After that, the sample was washed with distilled water until the pH is under 8. Before checking the structure is still complete as the MOR by XRD, the sample was dried at 100℃ in the oven overnight. Gone through the two round of ion exchange, the original sodium base MOR was changed to the ammonia base MOR, which gives more active sites than the original MOR.

For a better performance on bio-oil upgrading process, the ammonia MOR can still be ion exchanged by removing the ammonia from the structure, to change the ammonia base MOR to the hydrogen base MOR. To this end, the calcination with tube furnace was conducted on the sample to remove the ammonia as described above

3.3 CATALYST CHARACTERIZATION

3.3.1 POWDER X-RAY DIFFRACTION

Powder X-ray diffraction (XRD) was conducted under room temperature. The patterns were recorded on a BRUKER AXS D8 Advance diffractometer equipped with a Vantec-1 detector using Cu-K_α radiation ($\lambda = 1.5418$ Å) in flat plate geometry. The scanning range was from 0 degrees to 60 degrees 2θ for a duration of 20 minutes.

The unit cell parameters of the zeolite samples were calculated using the computer program called UnitCell.[70] This program assigned Millar indices to 2θ values from XRD patterns to calculate the unit cell parameters. All the data was recorded and input via normal text files.

3.3.2 SCANNING ELECTRON MICROSCOPY

Scanning electron microscopy (SEM) was used to obtain low-resolution micrographs via a JEOL SEM6480LV scanning electron microscope. The samples were prepared and evacuated for one day before undertaking the analysis. Also, to get better resolution images during the process, the samples were coated with gold

3.3.3 ENERGY DISPERSIVE X-RAY SPECTROMETRY

Energy dispersive X-ray spectrometry (EDX) was used to analyse the catalysts using an Oxford INCA X-ray analyser attached to the electron microscope with an acceleration voltage of 20 kV. The EDX data were collected via two different spectrum and three different points on each zeolite sample.

3.3.4 SOLID STATE MAGIC ANGLE SPINNING NUCLEAR MAGNETIC RESONANCE (SS MAS NMR)

For the solid state NMR, the Si and Al spectra were measured using a VARIAN VNMRS 400 spectrometer using direct excitation methods. Solid-state NMR spectra were collected at the EPSRC UK National Solid-state NMR Service at Durham. As the Na-FAU and H-FAU sample spectra are not very ideal, these two samples were re-analysed via a high resolution solid-state NMR spectrometer. The same operator and the same samples preformed the repeat spectra.

3.3.5 FOURIER TRANSFORM INFRARED SPECTOSCROPY

FT-IR spectra for the zeolite powder samples were recorded using a Perkin Elmer 100 FT-IR Spectrometer in the range 4000-600 cm^{-1}. One issue is the data below 650 cm^{-1} were not collected because of the instrumental limitations.

3.3.6 BET SURFACE AREA

To determine a catalyst's ability in bio-oil upgrading, one of the most important factors is its surface area. Therefore, the BET test was conducted on the zeolite catalyst samples to measure their surface area via nitrogen gas sorption measurement.

The samples were dried at 120℃ in the oven for at least 24 hours before conducting the surface area test. After the drying process, around 0.1 g of each of the samples was weighed and filled in the tubes to continue the surface area test with a set program. The tubes with sample have to be weighed when the test is finished, to get the difference between before experiment and after experiment.

The machine using for measuring the surface area of zeolite samples is 3Flex surface characterization analyzer. This machine is fully automatic with 3 channels connected with glass tubes that can test three different samples at one time. Firstly, the samples were placed in the tube for preparation, which mainly evacuates the air in the tube and measures the free space of samples before conducting the surface area measurement. After that, the test was conducted in a liquid nitrogen bath and nitrogen gas was filled into the tube to give a gas adsorption measurement over 24 hours. By recording the volume of nitrogen gas adsorption, surface area of samples can be calculated by the machine automatically.

3.4 CONVERSION OF MODEL BIO-OIL MIXTURE

3.4.1 MODEL OIL MIXTURE

Bio-oils mainly consist of aromatics, phenolics, aldehydes, carboxylic acids and ketones whereas hydrothermal liquefaction bio-oils have higher levels of aromatics and phenolics. In most experiments, model oils, defined as a small mixture of a few of these components are used to aid understanding of the mechanism and activity of certain catalysts [1, 5, 71].

The model mixture selected had a suitable proportion of double bonds, nitrogen content, oxygen content, acid and aromatics, which can simulate the HTL bio-oil to a good degree. The model mixture used in this study contained 17.3 wt% dodecylamine, 21.7 wt% pyrazine, 30.9 wt% oleic acid, 8.1 wt% 2,3,5-trimethylphenol and 22% dodecane.

Since the compounds are all solid phase at room temperature except oleic acid and dodecane, the mixture was very difficult to dissolve in homogeneous solution. Therefore, the model compounds were added separately to the batch reactors and mixed with catalyst to ensure the portion of each component is the same in every experiment.

3.4.2 MODEL BIO-OIL CONVERSION TESTING

For the conversion test, 1 g of model mixture and 0.1 g catalyst were added to a 6 mL stainless steel batch reactor without additional solvent. The reactors were sealed to prevent gas and liquid leak during the experiment. After sealing, the reactors were injected with 70 bar of nitrogen to check for leaks, this was released and the reactors further filled with 40 bar of hydrogen. Finally, the reactors were placed in the furnace to heat to 350 ℃, the reaction time was 2 hours. The reaction matrix is shown in table 2:

Table 2 Major components of HTL bio-oil produced with ethanol and water co-solvent, where R represents the ratio of ethanol and water mass. Reproduced from [13].

Runs	Time	R	W	Catalyst	W	T	H-P
1	2h	Model	1 g	FAU	0.1 g	350℃	40 bar
2	2h	Model	1 g	FAU	0.1 g	350℃	40 bar
3	2h	Model	1 g	FAU	0.1 g	350℃	40 bar
4	2h	Model	1 g	FAU (NH_4)	0.1 g	350℃	40 bar
5	2h	Model	1 g	FAU (NH_4)	0.1 g	350℃	40 bar
6	2h	Model	1 g	FAU (NH_4)	0.1 g	350℃	40 bar
7	2h	Model	1 g	FAU (H)	0.1 g	350℃	40 bar
8	2h	Model	1 g	FAU (H)	0.1 g	350℃	40 bar
9	2h	Model	1 g	FAU (H)	0.1 g	350℃	40 bar
10	2h	Model	1 g	MOR	0.1 g	350℃	40 bar
11	2h	Model	1 g	MOR	0.1 g	350℃	40 bar
12	2h	Model	1 g	MOR	0.1 g	350℃	40 bar
13	2h	Model	1 g	MOR (NH_4)	0.1 g	350℃	40 bar
14	2h	Model	1 g	MOR (NH_4)	0.1 g	350℃	40 bar
15	2h	Model	1 g	MOR (H)	0.1 g	350℃	40 bar
16	2h	Model	1 g	MOR (H)	0.1 g	350℃	40 bar
17	2h	Model	1 g	MOR (H)	0.1 g	350℃	40 bar
18	2h	Model	1 g	ZSM-5	0.1 g	350℃	40 bar
19	2h	Model	1 g	ZSM-5	0.1 g	350℃	40 bar
20	2h	Model	1 g	Blank	0.1 g	350℃	40 bar

After the conversion test at 350 ℃, the next stage was to conduct the conversion test at 300 ℃ to observe the conversion effects under

different temperature. To observe the effects of temperature, the reactions are designed the same as under 350℃ except the temperature was reduced to 300℃. The reaction matrix at 300℃ is shown in table 3:

Table 3 Reaction matrix 1, where R is reactant, W represents weight, T represents temperature and H-P is hydrogen pressure.

Runs	Time	R	W	Catalyst	W	T	H-P
1	2h	Model	1g	FAU	0.1g	300℃	40 bar
2	2h	Model	1g	FAU	0.1g	300℃	40 bar
3	2h	Model	1g	FAU (NH_4)	0.1g	300℃	40 bar
4	2h	Model	1g	FAU (NH_4)	0.1g	300℃	40 bar
5	2h	Model	1g	FAU (H)	0.1g	300℃	40 bar
6	2h	Model	1g	FAU (H)	0.1g	300℃	40 bar
7	2h	Model	1g	MOR	0.1g	300℃	40 bar
8	2h	Model	1g	MOR	0.1g	300℃	40 bar
9	2h	Model	1g	MOR (NH_4)	0.1g	300℃	40 bar
10	2h	Model	1g	MOR (NH_4)	0.1g	300℃	40 bar
11	2h	Model	1g	MOR (H)	0.1g	300℃	40 bar
12	2h	Model	1g	MOR (H)	0.1g	300℃	40 bar
13	2h	Model	1g	ZSM-5	0.1g	300℃	40 bar
14	2h	Model	1g	ZSM-5	0.1g	300℃	40 bar

After the conversion experiments, all the samples were washed with chloroform and analyzed with ^{1}H NMR analysis to determine the conversion. First of all, the samples were washed by chloroform via funnel with filter papers, and then samples were placed into the rota vapor to remove chloroform. At the end, the samples were sent to run the ^{1}H NMR test to determine the degree of conversion in each reaction.

4 RESULTS AND DISCUSSION

4.1 POWDER X-RAY DIFFRACTION

Powder X-ray diffraction (PXRD) was used to check the crystallinity and phase purity of the zeolite samples, which are zeolite-Y, mordenite and ZSM-5, by comparing their experimental patterns to their standard patterns from international zeolite association.[39, 42, 46] Normally, the peak positions match the standard pattern below 30 degrees; if so, the sample can be determined as the correct product.

To ensure the crystal structures match the standard pattern, the graphs below show the zeolite sample experimental pattern and standard pattern together in different types.

4.1.1 XRD of ZEOLITE-Y

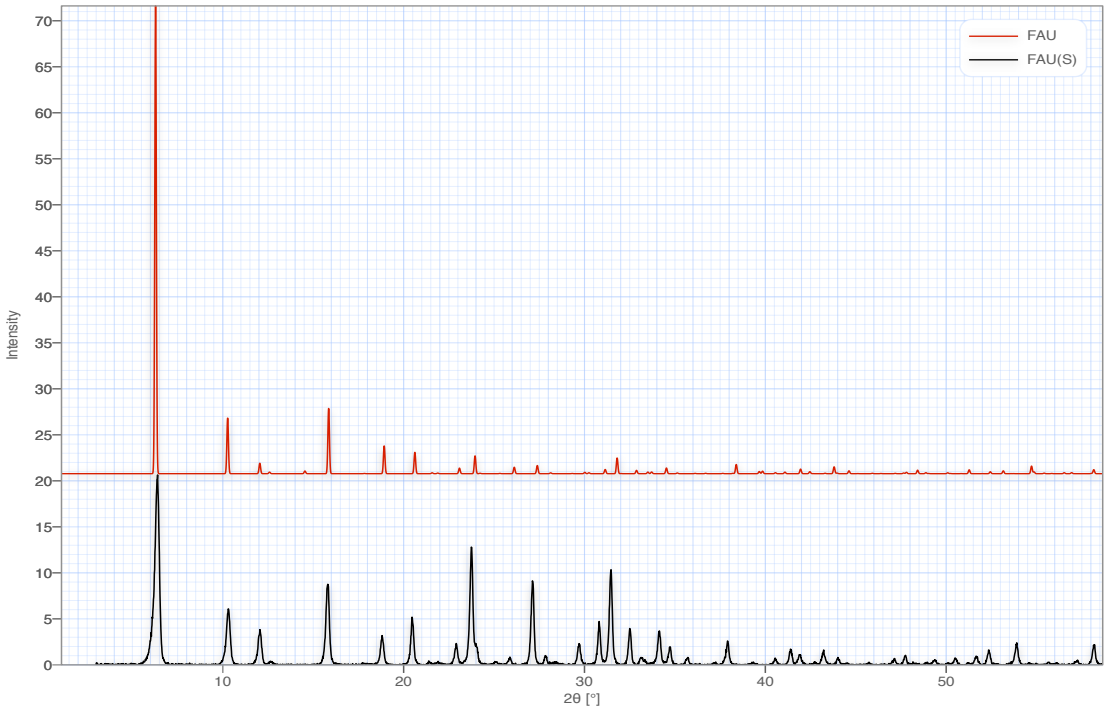

Figure 11 XRD of FAU in sodium base, where the black line represents pattern of FAU in sodium base and the red line is FAU standard pattern from international zeolite association.

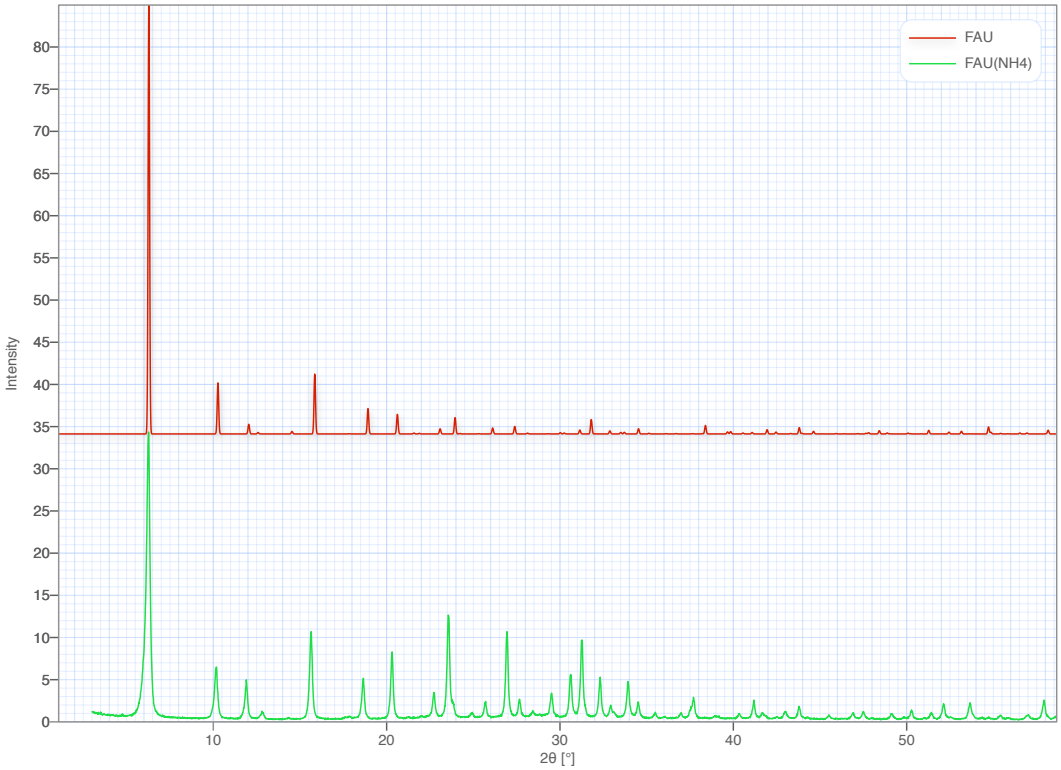

Figure 12 XRD of FAU in ammonia base, where the green pattern is FAU in ammonia base and red pattern is FAU standard pattern from international zeolite association.

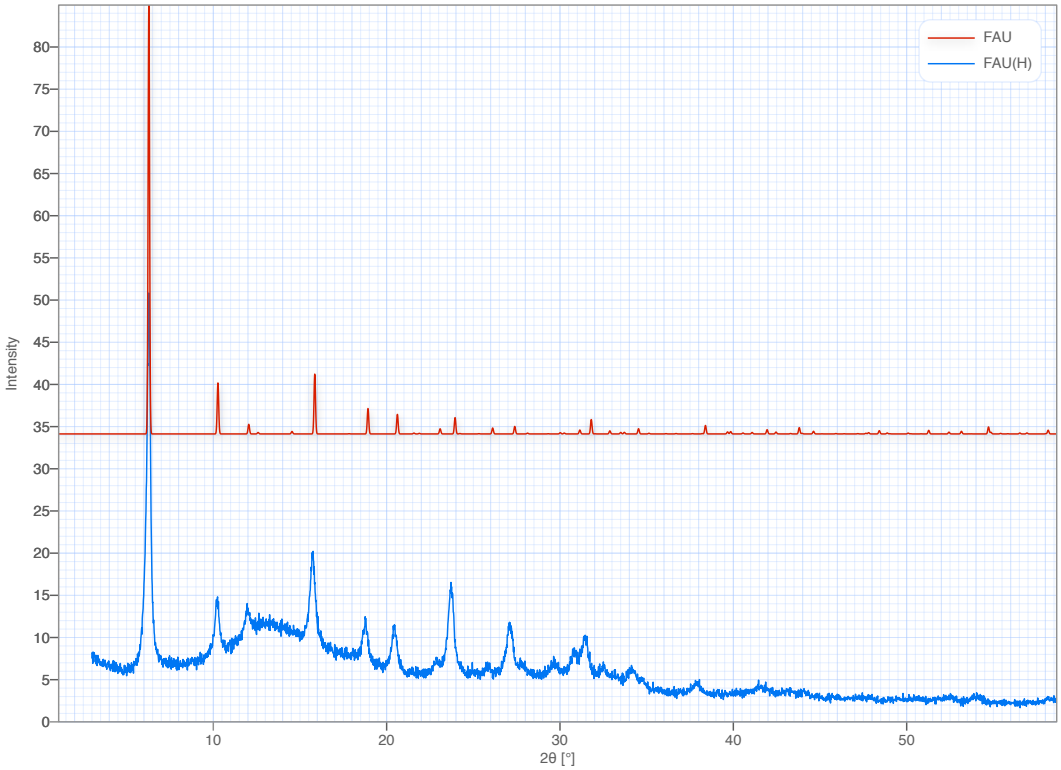

Figure 13 XRD of FAU in hydrogen base, the blue pattern is FAU in hydrogen base and red line represents the standard pattern of FAU from international zeolite association.

Figures 11, 12 and 13 show how the zeolite-Y samples, as-synthesized, ammonia exchanged and hydrogen base, are in agreement with the standard pattern. This means that the FAU framework is present throughout the samples. The fluctuations in hydrogen base zeolite-Y can be caused by the calcination step, since the removal of ammonia might cause the structure to squeeze in a small range. As the ammonia ions bond with aluminum were removed by high temperature, the hydrogen ions left replaced ammonia ions have a smaller particle size, the framework of zeolite particles could be squeezed slightly. Therefore, the difference of particle size presents as fluctuations in the graph.

4.1.2 XRD OF MORDENITE

The next series of spectra compare the mordenite experimental patterns to its standard pattern.

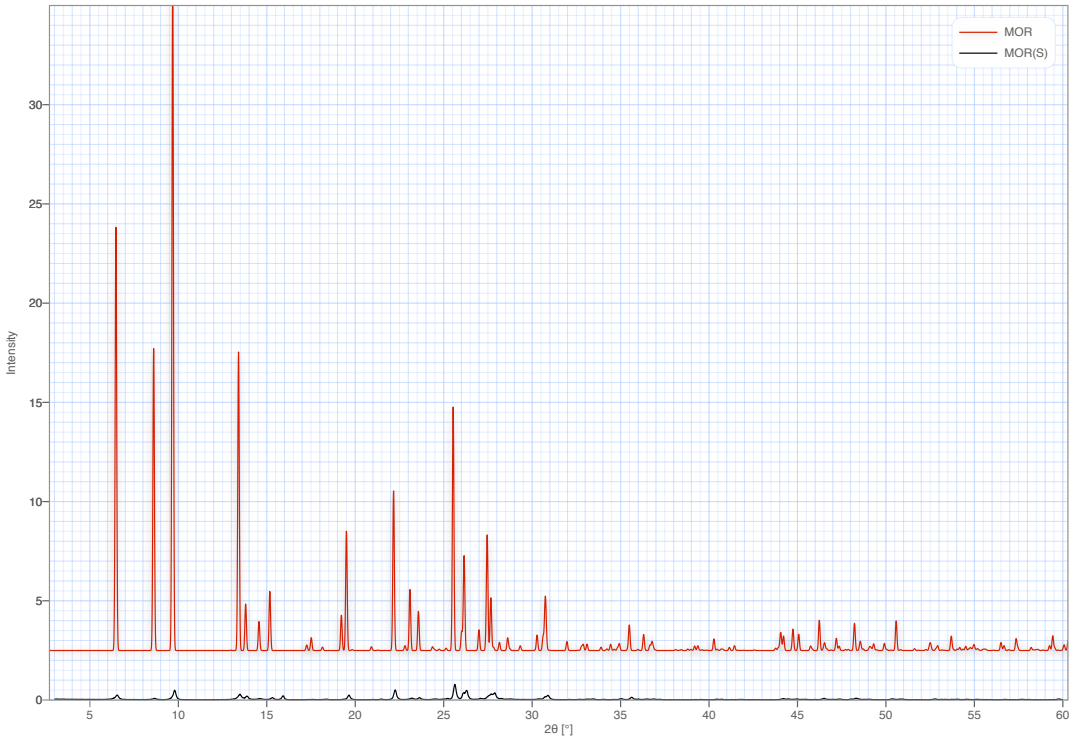

Figure 14 XRD of MOR in sodium base, the black line is pattern of MOR in sodium base and the red line is MOR standard pattern from international zeolite association.

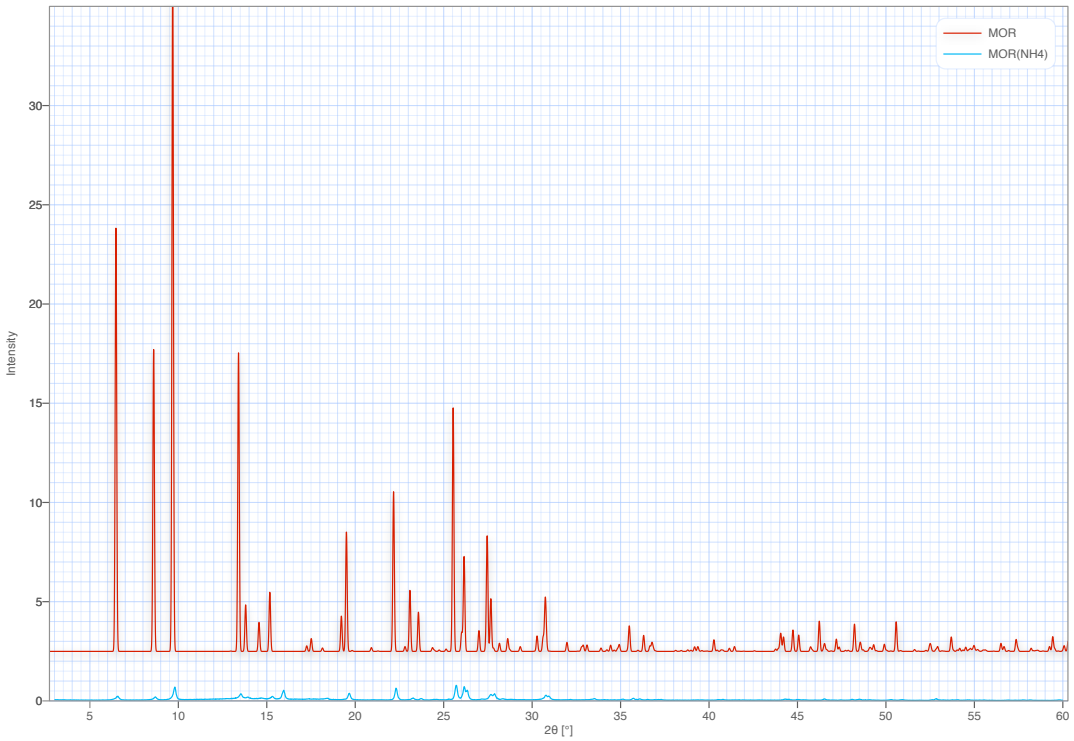

Figure 15 XRD of MOR in ammonia base, the blue line shows pattern of MOR in ammonia base and the red line is MOR standard pattern from international zeolite association.

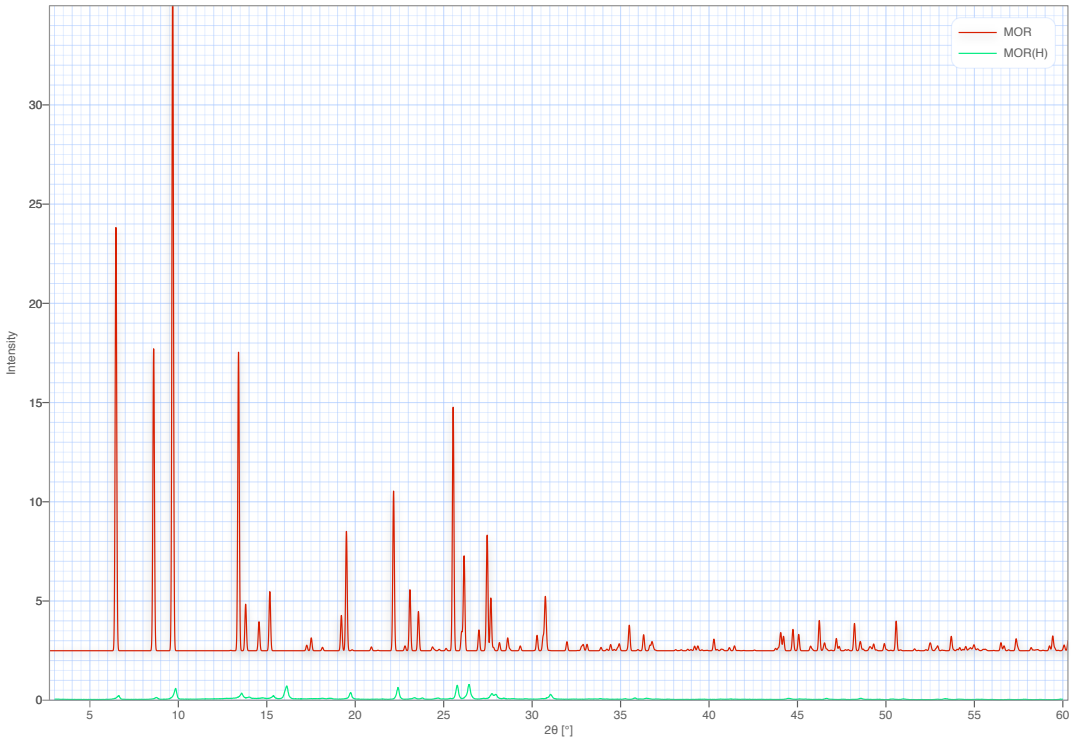

Figure 16 XRD of MOR in hydrogen base, the green pattern is MOR in hydrogen base and the red pattern is MOR standard pattern from international zeolite association.

From the spectrums of mordenite, there is a good agreement between the experimental patterns and the standard. However, an obvious issue is the purity of MOR is not ideal, since some of its peaks are not in the exact same positions as the standard pattern. It may caused by the temperature of synthesis, as the lower temperature (less than 190℃) cannot get fully formed zeolite, so the temperature was set at 190℃ for a complete crystallization, which generated a small amount of other types of crystals. Therefore, it seems that the MOR sample is not entirely one type.

4.1.3 **XRD OF ZSM-5**

The XRD pattern of the ZSM-5 was recorded and compared to the standard pattern (figure 17).

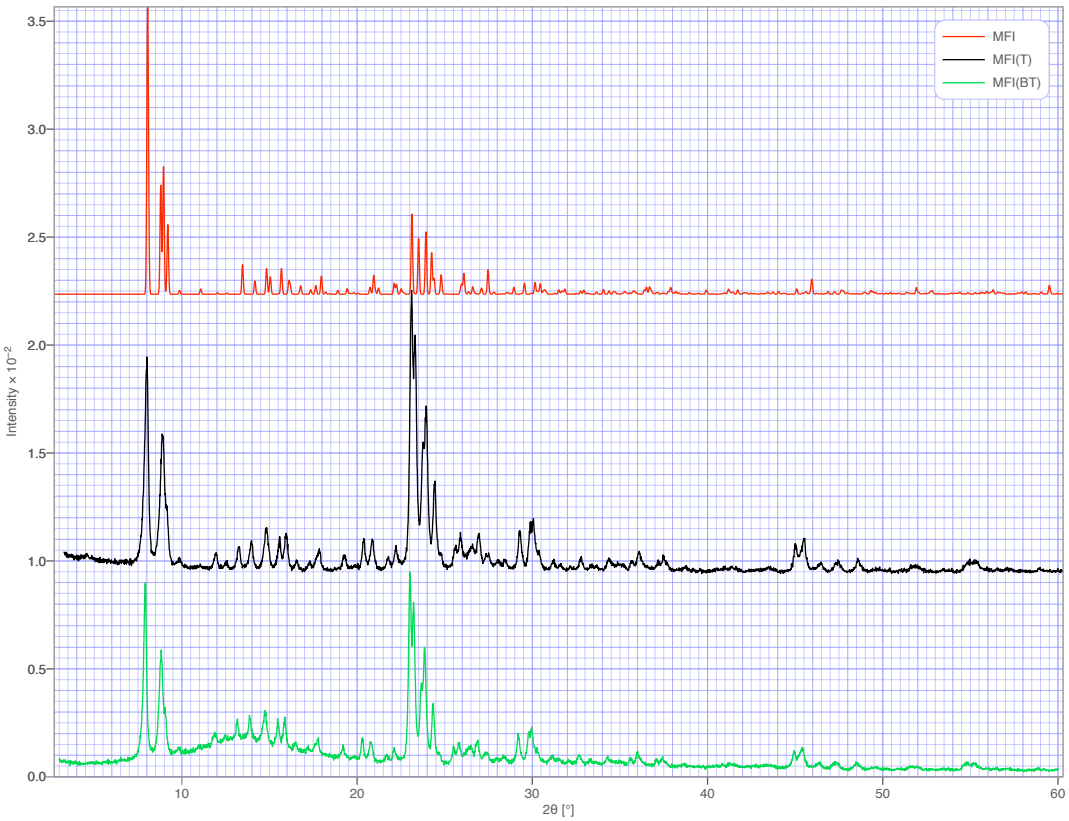

Figure 17 XRD of ZSM-5, the red pattern is standard pattern of ZSM-5 (MFI) from international zeolite association, the black pattern is ZSM-5 synthesized with template (need to be removed) and the green pattern represents the template removed ZSM-5 by calcination.

Based on the spectrums of ZSM-5, it is shown that the ZSM-5 experimental pattern agrees with the standard pattern before and after removing the TPA-OH template. Here, the MFI represents ZSM-5, MFI (T) is ZSM-5 with TPA-OH template and MFI (BT) is ZSM-5 without TPA-OH. The ZSM-5 does not change during the calcination process, and therefore seemingly has kept its crystalline structure.

4.1.4 CELL PARAMETER OF ZEOLITES

According to the experimental patterns, the 2θ values at peak positions can be recorded to index every peak and get the indexing values (h, k, l values) via the data sheets of every type of zeolite crystals [72-74]. The indexing peak graphs of FAU zeolite sample is shown in figure 18:

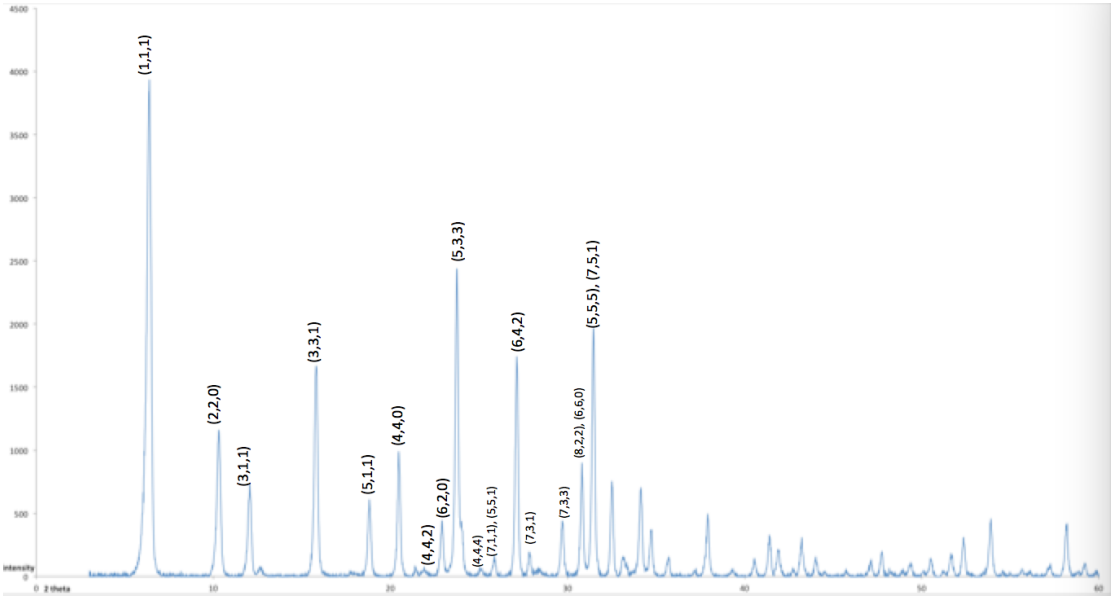

Figure 18 Indexing peaks of FAU (Na), the indexing parameter is from [72, 75].

Base on the indexing values and the 2θ values, the crystal size can be calculated by equation (2) the Scherrer calculation. The Scherrer equation is just a value of assessment, so the results need to be double checked by the actual crystal size that can be measured by the program named Image J. The results of crystal size are shown in table 4:

Table 4 Crystal sizes of Scherrer equation calculation and Image J measurement.

Samples	Max peak	Size/nm	Image J	Size/nm
Na-FAU	(1, 1, 1)	60.7		112.264
NH4-FAU	(1, 1, 1)	64.86		150
H-FAU	(1, 1, 1)	57.9		123.65
Na-MOR	(2, 0, 2)	94.96		1570.618
NH4-MOR	(2, 0, 2)	96.12		2115.906
H-MOR	(2, 0, 2)	96.38		1869.582
ZSM-5	(0, 5, 1)	63.4		2704.084

The crystal sizes of the FAU zeolites become larger when the ions change to NH_4, and smaller than the original sodium base when Na is replaced with H^+. This phenomenon indicates that the structure of crystals are enlarged firstly, and squeezed later when the ion change to hydrogen. However, there is a big difference between the results from the Scherrer calculation and image J in MOR and ZSM-5 samples, it might because the Scherrer equation is only for underestimating average value of crystal size and cannot match a particular particle

size screened by SEM.[75]

The peak positions can be found by using excel program. With the peak positions' values and peak indexes, the cell parameters can be calculated by the computer program UnitCell[70]. Based on this method, all the cell parameters can be calculated. The results are shown in table 5:

Table 5 Cell parameters of zeolite samples, sd represents standard deviation.

Catalyst	a	b	c	sd (2T)
Na-FAU	24.58			0.077
NH_4-FAU	24.67			0.099
H-FAU	24.63			0.075
Na-MOR	18.10	20.48	7.52	0.037
NH_4-MOR	18.10	20.46	7.50	0.057
H-MOR	18.03	20.38	7.48	0.064
ZSM-5	19.87	20.12	13.38	0.036

Since FAU is cubic crystal, it only has value a. from the table of cell parameter, it can be seen that the data is quite similar in the same type of zeolite, so it indicates the crystal structures does not change after the ion exchange.

4.2 SCANNING ELECTRON MICROSCOPY

The SEM pictures give a solid reference of the crystal structure of zeolite samples via different magnitude.

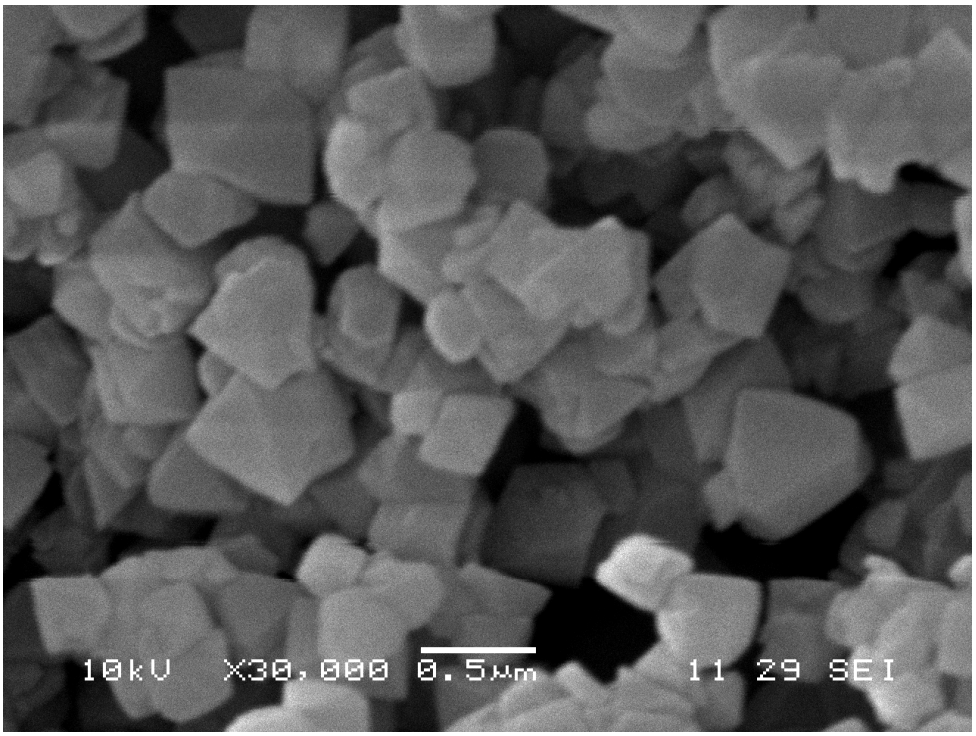

Figure 19 SEM picture of FAU (Na)

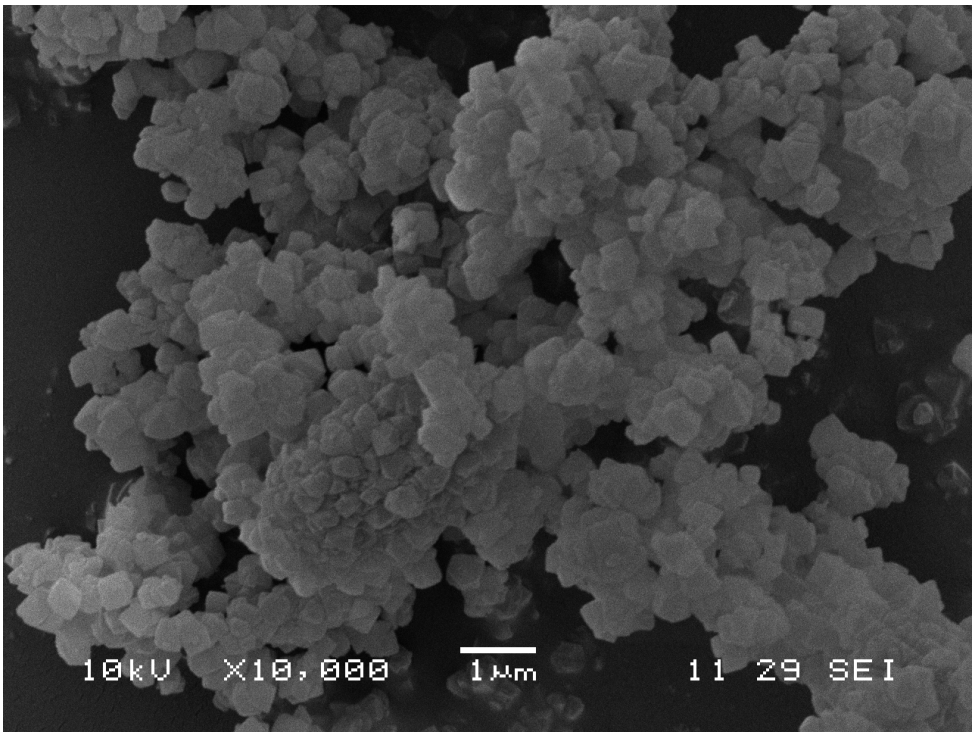

Figure 20 SEM picture of FAU (NH_4)

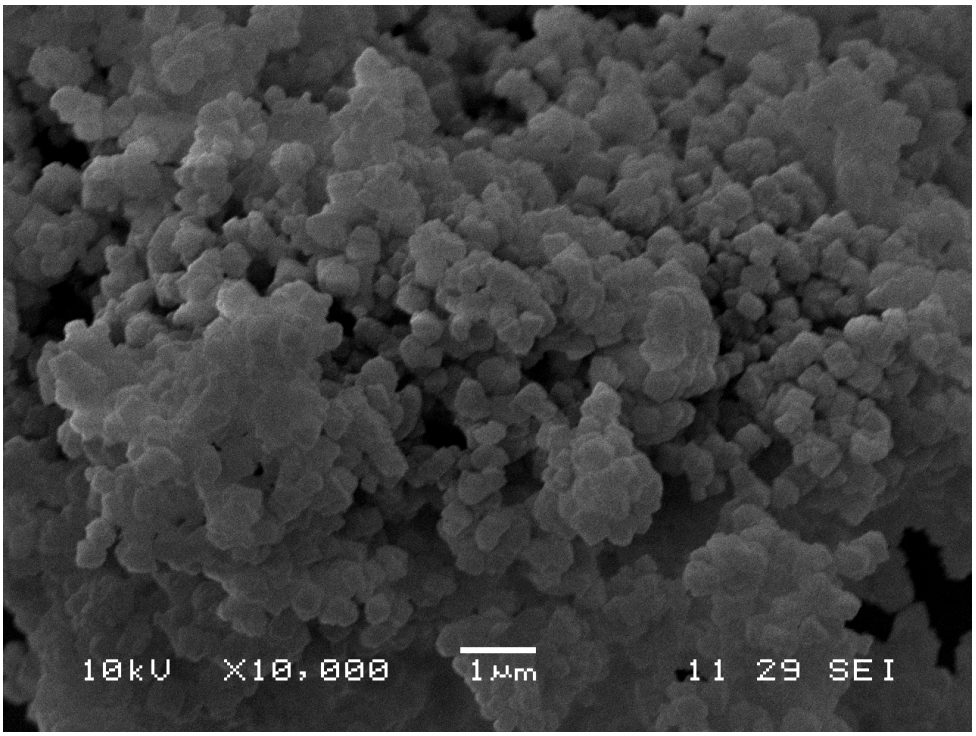

Figure 21 SEM picture of FAU (H)

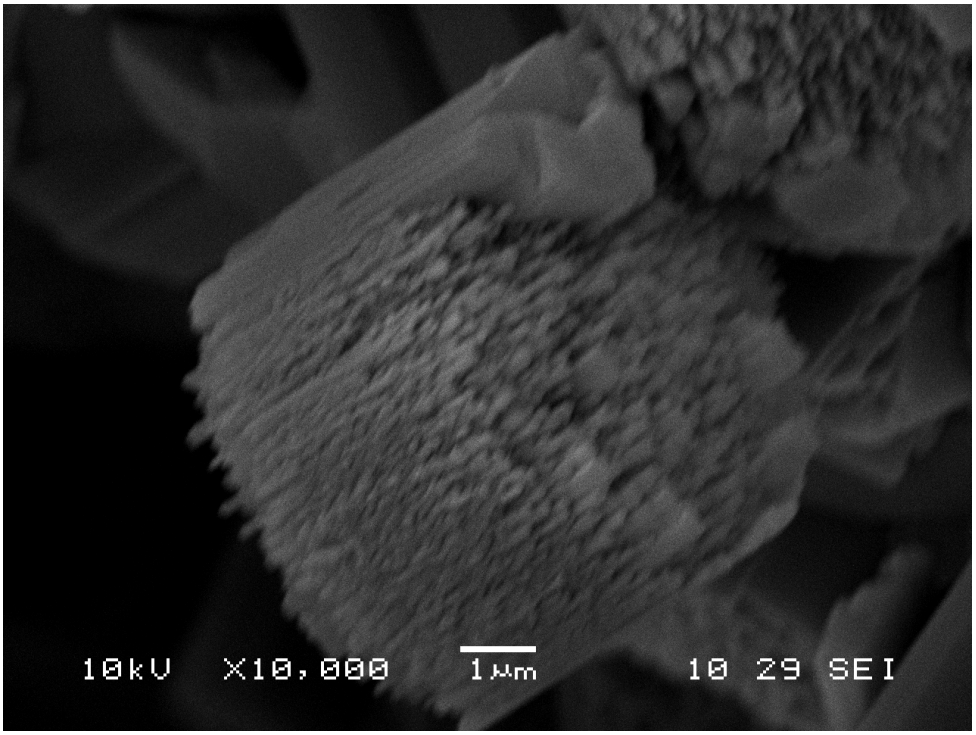

Figure 22 SEM picture of MOR (Na)

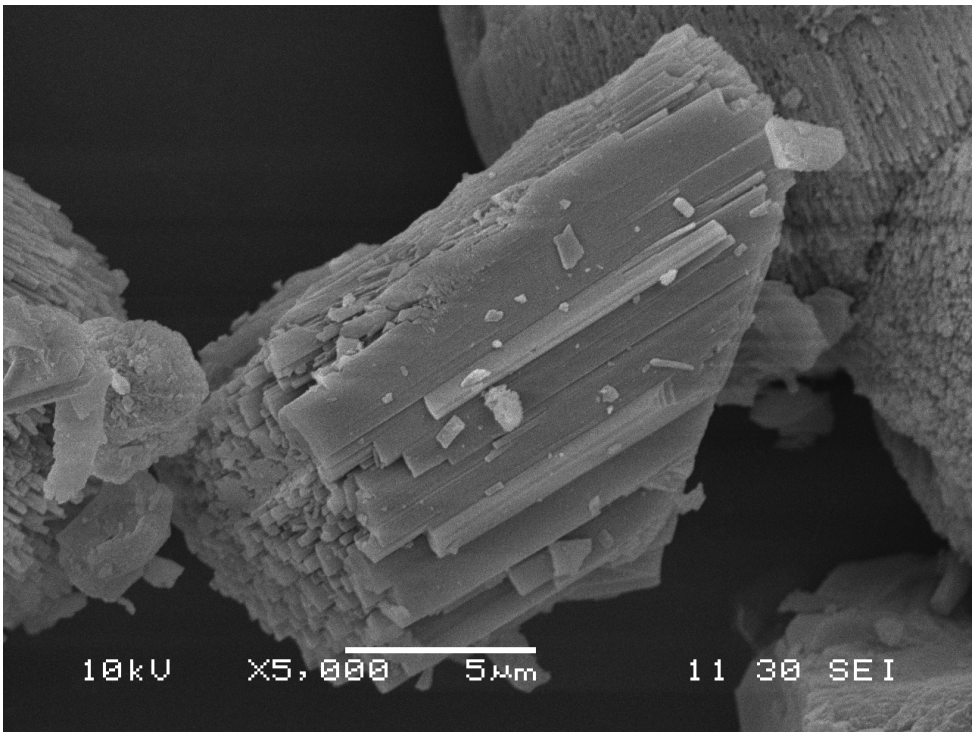

Figure 23 SEM picture of MOR (NH_4)

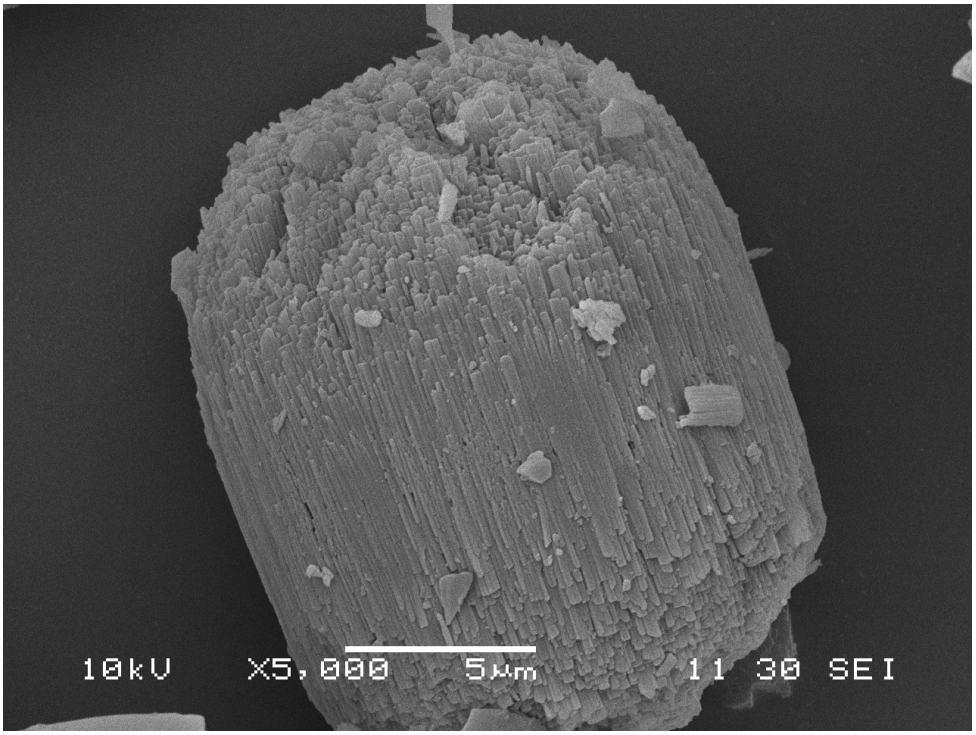

Figure 24 SEM of picture of MOR (H)

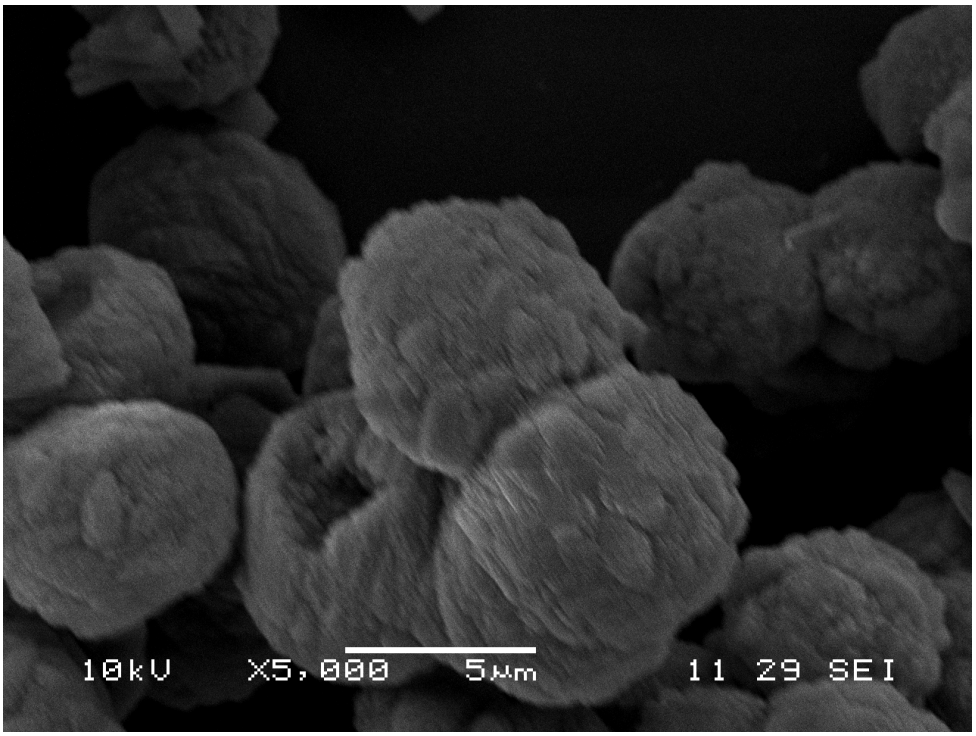

Figure 25 SEM picture of ZSM-5

According to the SEM pictures, FAU in all different bases show a cubic structure in single particle, and attached closely in a large group. However, it can be seen that the distance between particles was keeping decreasing from sodium base to hydrogen base, which indicates there is a slight squeeze during ion exchange. With this structure, FAU provides micro pores around its surface and mesopores between every particle, which can give more accesses for different size of molecules and attach more molecules than separate zeolite particles.

MOR particles in all different bases present a cylinder shape, the pores in MOR was enlarged to tunnels. With the sodium base MOR was changing to hydrogen base, the length of particles and density of pores were increasing. This phenomenon indicates ion exchange also caused a squeeze on particle structure, which elongated MOR particles and gave particles more intensive distribution of pores. Compared with FAU, MOR has larger particle size and large pore size, which let the small molecules can go through the MOR particle more easily. Another difference is MOR distributes separately instead of attaching together.

ZSM-5 has a hemispheroidal shape with pores around its surface, and attached in a small group. This structure makes mesopores between single ZSM-5 particles. Although, ZSM-5 has quite similar distribution to FAU, it only attaches in small group, so it cannot make as many

pores as FAU. Moreover, the larger pore size and particle size determine ZSM-5 cannot attach the same size molecules as FAU.

4.3 ENERGY DISPERSIVE X-ray SPECTROMETRY

The EDX analysis gives a rough elemental analysis of the zeolite samples (table 6 to 12).

Table 6 EDX of FAU (Na)

Spectrum	In stats.	C	O	Na	Al	Si	Total	Si/Al
Spectrum 1	Yes	17.62	41.52	6.66	11.29	22.91	100	2.0
Spectrum 2	Yes	10.34	41.25	7.97	13.4	27.04	100	2.0
Spectrum 3	Yes	16.1	46.62	6.85	10.12	20.3	100	2.0
Mean		14.69	43.13	7.16	11.61	23.42	100	2.0
Std. deviation		3.84	3.03	0.71	1.66	3.4		
Max.		17.62	46.62	7.97	13.4	27.04		
Min.		10.34	41.25	6.66	10.12	20.3		

Table 7 EDX of FAU (Na)

Spectrum	In stats.	C	O	Na	Al	Si	Total	Si/Al
Spectrum 1	Yes	13.07	44.65	2.2	13.34	26.75	100	2.0
Spectrum 2	Yes	14.48	47.27	2.04	11.87	24.34	100	2.1
Spectrum 3	Yes	15.87	48.15	2.08	11.6	22.29	100	1.9
Mean		14.47	46.69	2.11	12.27	24.46	100	2.0
Std. deviation		1.4	1.83	0.08	0.93	2.23		
Max.		15.87	48.15	2.2	13.34	26.75		
Min.		13.07	44.65	2.04	11.6	22.29		

Table 8 EDX of FAU (H)

Spectrum	In stats.	C	O	Na	Al	Si	Total	Si/Al
Spectrum 1	Yes	6.66	45.96	2.87	14.65	29.85	100	2.0
Spectrum 2	Yes	8.23	51.45	2.4	12.82	25.1	100	2.0
Spectrum 3	Yes	5.61	50.23	2.47	13.71	27.99	100	2.0
Spectrum 4	Yes	6.29	48.73	2.31	14.04	28.63	100	2.0
Mean		6.7	49.09	2.51	13.8	27.89	100	2.0
Std. deviation		1.11	2.37	0.25	0.76	2.02		
Max.		8.23	51.45	2.87	14.65	29.85		
Min.		5.61	45.96	2.31	12.82	25.1		

Table 9 EDX of MOR (Na)

Spectrum	In stats.	Na	Al	Si	Total	Si/Al
Spectrum 1	Yes	6.07	11.34	82.58	100	7.282186949
Spectrum 2	Yes	4.92	12.74	82.34	100	6.46310832
Spectrum 3	Yes	7.22	11.58	81.19	100	7.011226252
Spectrum 4	Yes	3.93	11	85.07	100	7.733636364
Mean		5.54	11.67	82.8	100	7.122539471
Std. deviation		1.43	0.76	1.63		
Max.		7.22	12.74	85.07		
Min.		3.93	11	81.19		

Table 10 EDX of MOR (NH_4)

Spectrum	In stats.	Na	Al	Si	Total	Si/Al
Spectrum 1	Yes	3.95	19.13	76.92	100	4.020909566
Spectrum 2	Yes	0.27	13.06	86.67	100	6.636294028
Spectrum 3	Yes	0.01	12.1	87.89	100	7.263636364
Spectrum 4	Yes	0.38	15.25	84.36	100	5.531803279
Mean		1.15	14.89	83.96	100	5.863160809
Std. deviation		1.87	3.12	4.92		
Max.		3.95	19.13	87.89		
Min.		0.01	12.1	76.92		

Table 11 EDX of MOR (H)

Spectrum	In stats.	Na	Al	Si	Total	Si/Al
Spectrum 1	Yes	0.84	11.84	87.32	100	7.375
Spectrum 2	Yes	0.71	12.53	86.76	100	6.924181963
Spectrum 3	Yes	1.33	11.14	87.52	100	7.856373429
Spectrum 4	Yes	0.17	13.58	86.25	100	6.351251841
Mean		0.76	12.27	86.96	100	7.126701808
Std. deviation		0.48	1.04	0.57		
Max.		1.33	13.58	87.52		
Min.		0.17	11.14	86.25		

Table 12 EDX of ZSM-5

Spectrum	In stats.	Na	Al	Si	Total	Si/Al
Spectrum 1	Yes	1.26	4.34	94.4	100	21.75115207
Spectrum 2	Yes	1.03	3.44	95.52	100	27.76744186
Spectrum 3	Yes	2.1	5.6	92.3	100	16.48214286
Mean		1.81	3.53	94.66	100	22.0002456
Std. deviation		0.83	2.06	1.78		
Max.		2.84	5.6	96.41		
Min.		1.03	0.74	92.3		

According to the results, the FAU samples in different bases shows a very good stability in Si/Al ratio at around 2, and they are also close to the ratio from the recipe, which are 2.4 for standard. These results reflect the SEM pictures very well, since the structure of FAU in different bases just has a slight change. However, the MOR and ZSM-5 do not have very stable results in Si/Al ratio. The MOR has the results located around 7, which is lower than the 9 in standard. This can be caused by the crystals not forming properly, since the SEM pictures shows there are some small particles among MOR particles have quite different shapes, which could be the unformed MOR particles. For the ZSM-5, the results are located in the range from 16 to 27, which are much higher than the standard ratio 13. This means the ZSM-5 sample only has a tiny portion of aluminum. ZSM-5 just attached in small groups in the SEM pictures; the big difference could be caused by the asymmetric distribution.

4.4 SOLID STATE MAGIC ANGLE SPINNING NUCLEAR MAGNETIC RESONANCE (SS MAS NMR)

Solid-state NMR is very sensitive to the elemental environment and analysis; the Si/Al ratio can also be obtained from this method via graph fitting. Another important result can get from this method is Si chemical shifts in different environment.

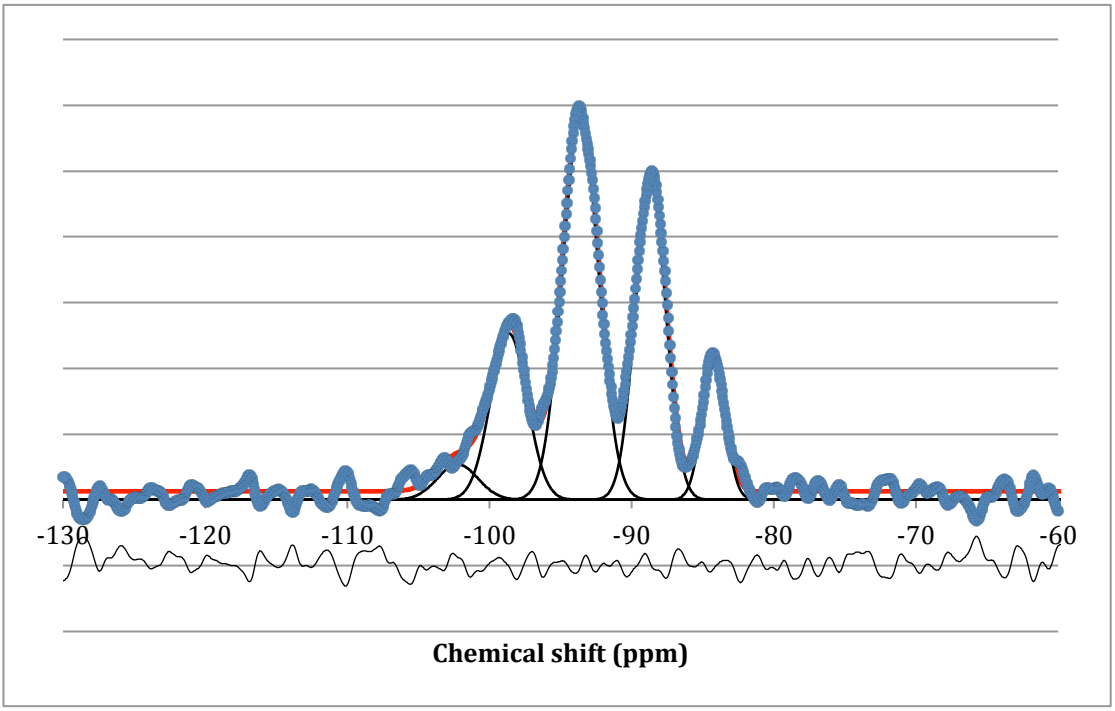

Figure 26 SS NMR fitting of FAU (Na), where the blue line is observe line, the red line is fitting line, the black line at the bottom represents the difference line, the bold black peaks are fitting peaks.

Figure 26 shows the Si SS NMR fitting, the observe line drawn by data from SS NMR, the fitting line is drawn by calculated results, the black line at the bottom is difference between observe line and fitting line, and the five peaks represents the Si ions in different environment, which attached the amount of Al atoms from 0 to 4, from right to left of chemical shift axis.

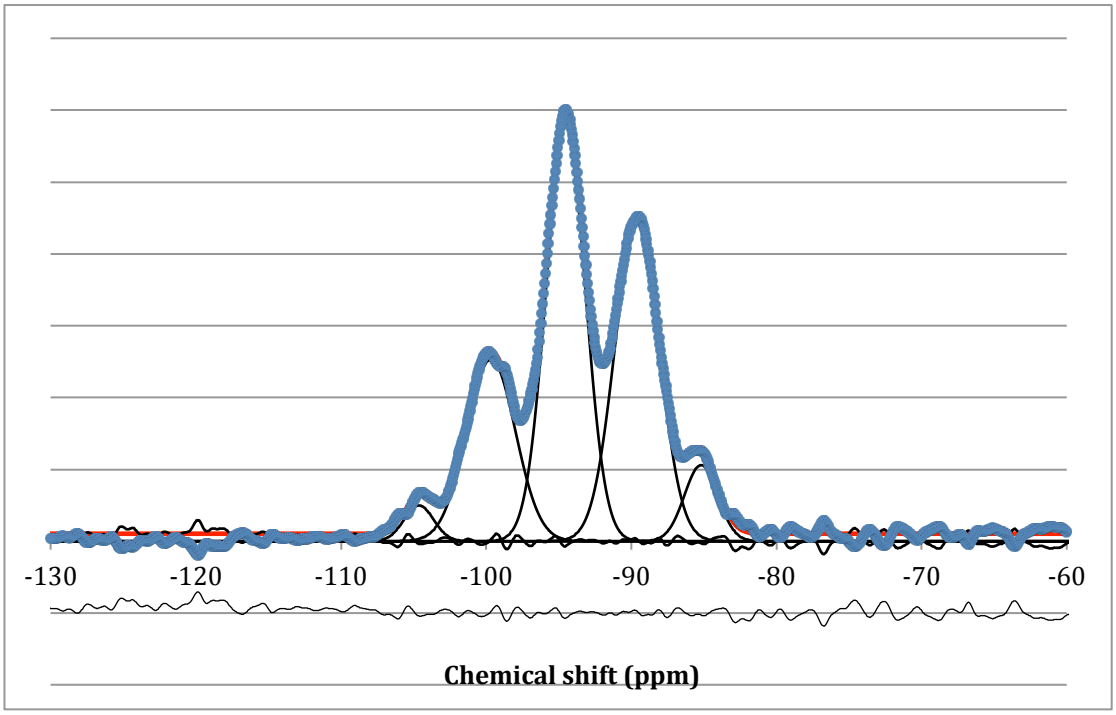

Figure 27 SS NMR fitting of FAU (NH_4), where the blue line is observe line, the red line is fitting line, the black line in the bottom represents the difference line, the bold black peaks are fitting peaks.

Figure 27 shows the Si SS NMR fitting, the observe line drawn by data from SS NMR, the fitting line is drawn by calculated results, the black line at the bottom is difference between observe line and fitting line, and the five peaks represents the Si ions in different environment, which attached the amount of Al atoms from 0 to 4, from right to left of chemical shift axis.

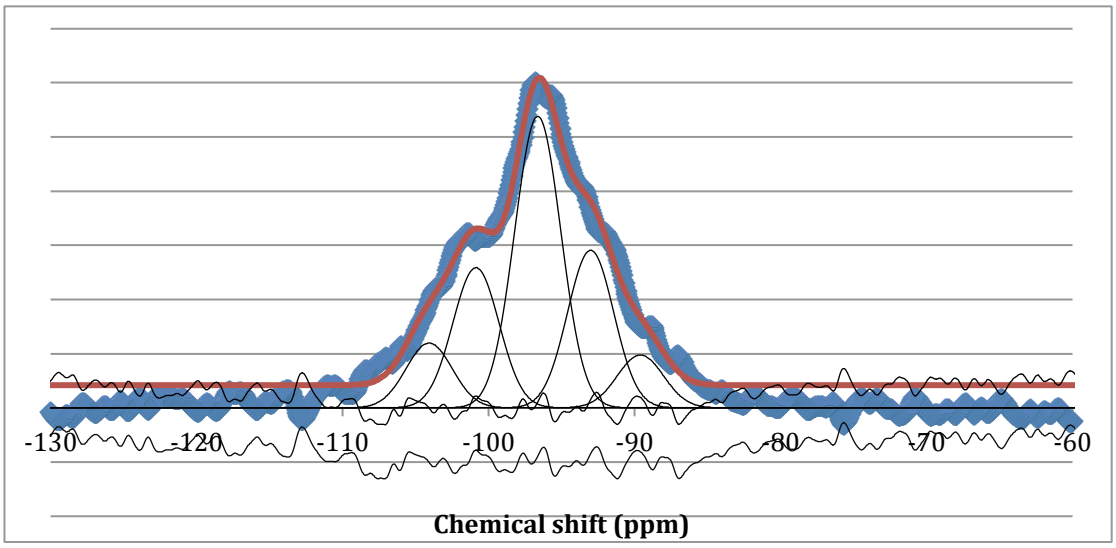

Figure 28 SS NMR of FAU (H), where the blue line is observe line, the red line is fitting line, the black line in the bottom represents the difference line, the above line is mismatch line, and the bold black peaks are fitting peaks.

Figure 28 indicates the Si SS NMR fitting, the observe line drawn by data from SS NMR, the fitting line is drawn by calculated results, the black line at the bottom is difference between observe line and fitting line, the black line above difference is mismatch line between observe line and fitting line, and the five peaks represents the Si ions in different environment, which attached the amount of Al atoms from 0 to 4, from right to left of chemical shift axis.

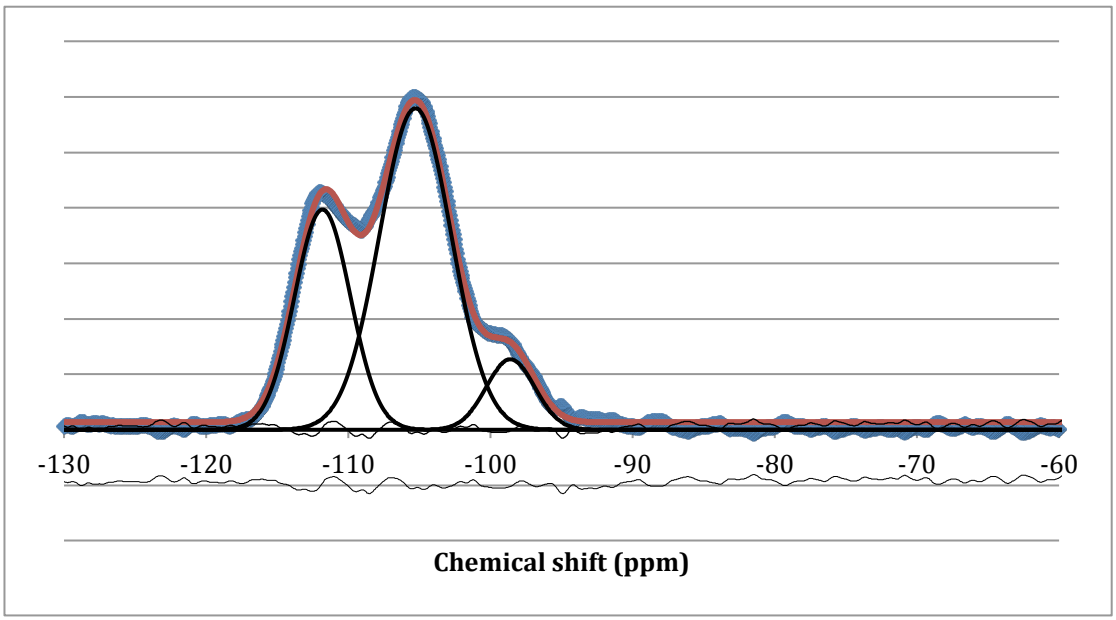

Figure 29 SS NMR of MOR (Na), where the blue line is observe line, the red line is fitting line, the black line in the bottom represents the difference line, the above line is mismatch line, and the bold black peaks are fitting peaks.

Figure 29 presents the Si SS NMR fitting, the observe line drawn by data from SS NMR, the fitting line is drawn by calculated results, the black line at the bottom is difference between observe line and fitting line, the black line above difference is mismatch line between observe line and fitting line, and the three peaks represents the Si ions in different environment, which attached the amount of Al atoms from 2 to 4, from right to left of chemical shift axis.

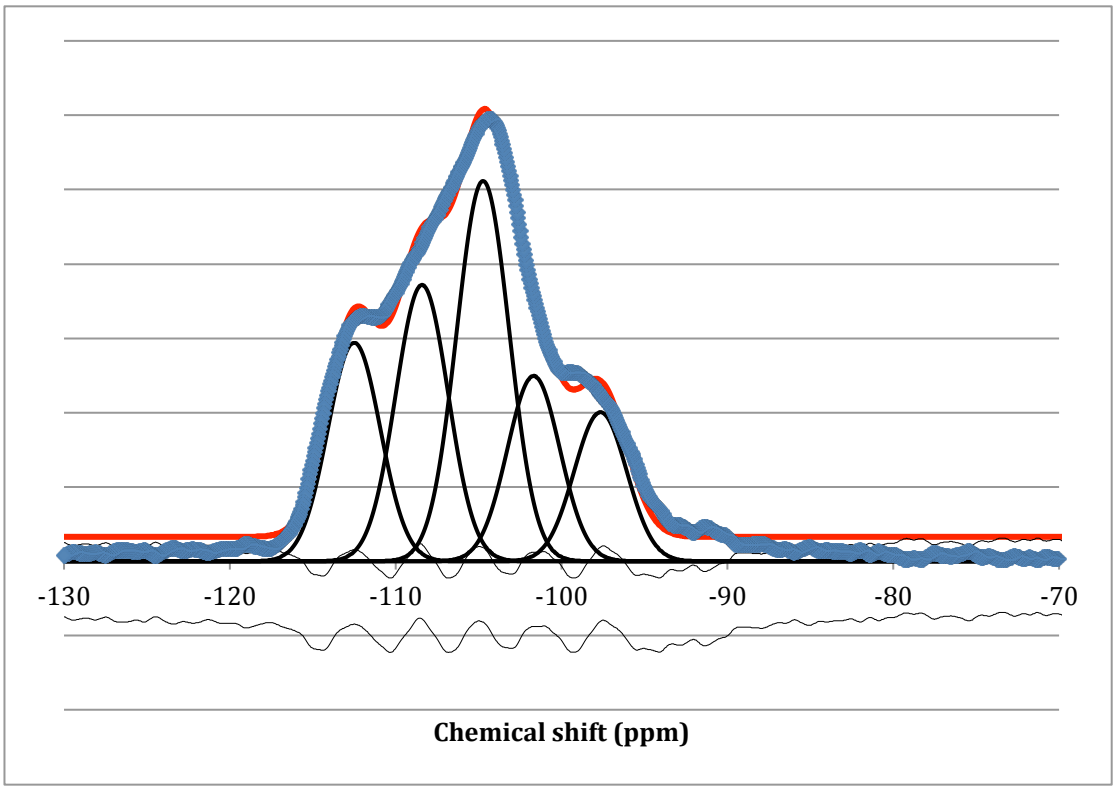

Figure 30 SS NMR of MOR (NH_4), where the blue line is observe line, the red line is fitting line, the black line in the bottom represents the difference line, the above line is mismatch line, and the bold black peaks are fitting peaks.

Figure 30 indicates the Si SS NMR fitting, the observe line drawn by data from SS NMR, the fitting line is drawn by calculated results, the black line at the bottom is difference between observe line and fitting line, the black line above difference is mismatch line between observe line and fitting line, and the five peaks represents the Si ions in different environment, which attached the amount of Al atoms from 0 to 4, from right to left of chemical shift axis.

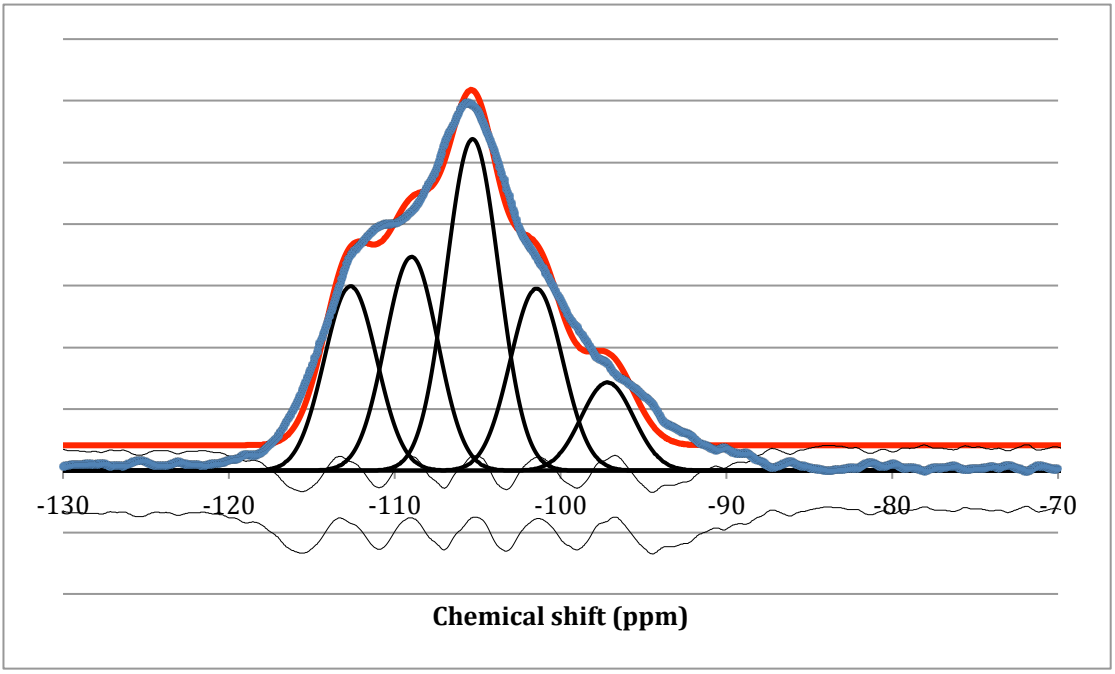

Figure 31 SS NMR of MOR (H), where the blue line is observe line, the red line is fitting line, the black line in the bottom represents the difference line, the above line is mismatch line, and the bold black peaks are fitting peaks.

Figure 31 shows the Si SS NMR fitting, the observe line drawn by data from SS NMR, the fitting line is drawn by calculated results, the black line at the bottom is difference between observe line and fitting line, the black line above difference is mismatch line between observe line and fitting line, and the five peaks represents the Si ions in different environment, which attached the amount of Al atoms from 0 to 4, from right to left of chemical shift axis.

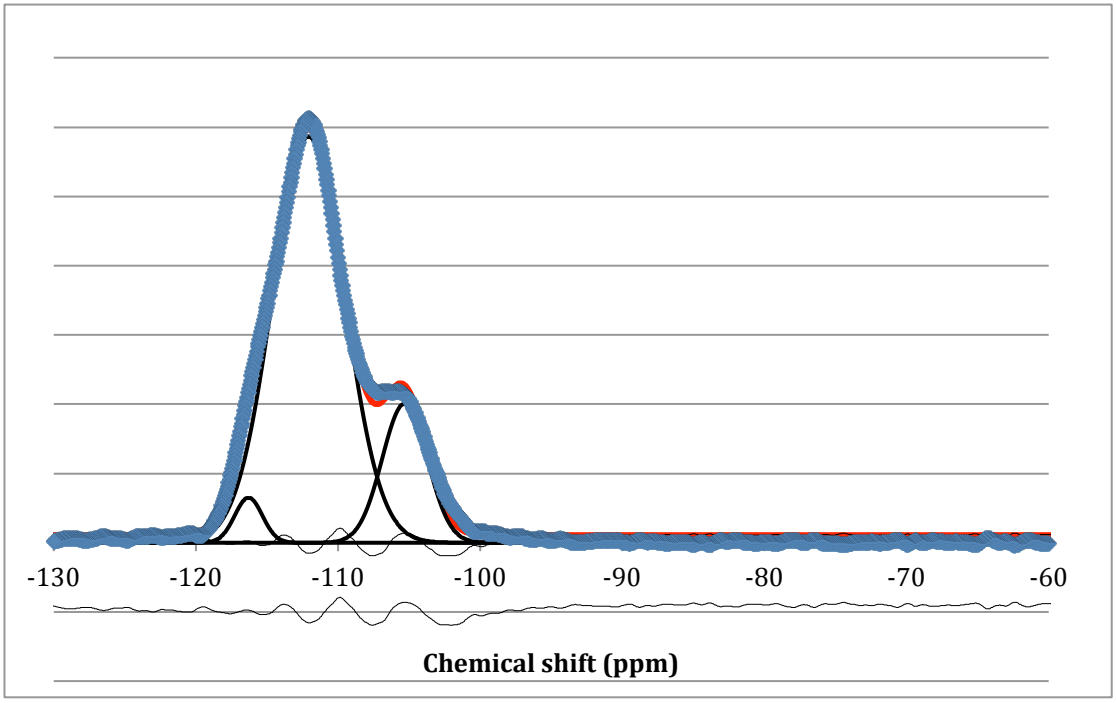

Figure 32 SS NMR of ZSM-5, where the blue line is observe line, the red line is fitting line, the black line in the bottom represents the difference line, the above line is mismatch line, and the bold black peaks are fitting peaks.

Figure 32 gives the Si SS NMR fitting, the observe line drawn by data from SS NMR, the fitting line is drawn by calculated results, the black line at the bottom is difference between observe line and fitting line, the black line above difference is mismatch line between observe line and fitting line, and the three peaks represents the Si ions in different environment, which attached the amount of Al atoms from 2 to 4, from right to left of chemical shift axis.

From the solid state NMR spectrums, the Si fitting peaks areas can be obtained by changing the underestimate area of peaks to fit observe line and fitting line, according the peaks areas, the Si/Al ratio can be calculated from the spectrums (table 13 and 14).

Table 13 Fitting peaks and Si/Al ratio, where the 0Al-4Al represents the Si bonded with the amount of Al from 0 to 4. The Si/Al ratio was calculated by summation of all peak areas divided by the summation of each peak area times ratio of amount of Al and 4.

Si peaks area	Na-FAU	NH_4-FAU	H-FAU	Na-MOR	NH_4-MOR	H-MOR	ZSM-5
0Al	38.49	25.31	94.77	390.88	233.15	237.19	0
1Al	162.48	213.36	205.05	734.04	294.63	274.95	0
2Al	372.11	394.17	426.47	108.48	405.54	426.44	31.62
3Al	261.06	339.19	230.48	0	158.94	234.13	743.64
4Al	84.65	60.71	77.45	0	197.68	113.47	159.13
Si/Al ratio	1.81	1.83	2.01	5.19	2.17	2.25	1.28

Table 14 Si peaks of samples

	0Al	1Al	2Al	3Al	4Al
Na-FAU	-84.2	-88.7	-93.6	-98.7	-102.3
NH_4-FAU	-85.2	-89.6	-94.5	-99.7	-104.6
H-FAU	-89.6	-93	-96.6	-100.9	-104.1
Na-MOR	0	0	-98.6	-105.3	-111.8
NH_4-MOR	-97.7	-101.7	-104.7	-108.4	-112.5
H-MOR	-97.2	-101.5	-105.3	-109	-112.7
ZSM-5	0	0	-105.3	-112.1	-116.3

According to the results, the Si/Al ratios are quite different from data acquired from EDX, since the EDX is just a rough elemental analysis, the SS NMR should be more accurate. For the increase of Si chemical shifts, it can be explained as the structures of samples are expanded after the ion exchange.

Another characterization parameter can be obtained from the solid state NMR is the T-O-T angles. According to the equation (3), the results can be calculated and shown as follow:

Table 15 T-O-T angles of zeolites sample

	Si (2Al)
Na-FAU	155.04
NH4-FAU	156.61
H-FAU	159.95
Na-MOR	175.56
NH4-MOR	173.46
H-MOR	167.84
ZSM-5	176.61

From the results, it can be seen that the T-O-T angles of FAU are decreasing, since the structure of FAU is enlarging with the ion

exchange process. On the other hand, the structure of MOR is squeezing during the ion exchange.

4.5 FT-IR

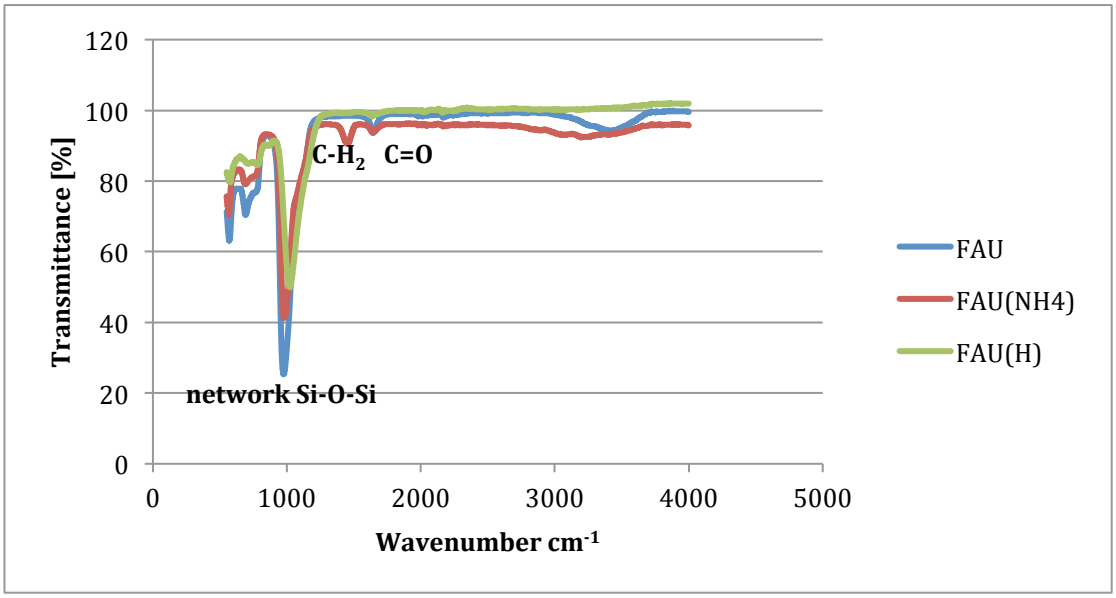

Figure 33 FT-IR of FAU, the major peaks are labeled as in the graph, the peaks between 3000 an 4000 is undetected, which could be ethanol solution.

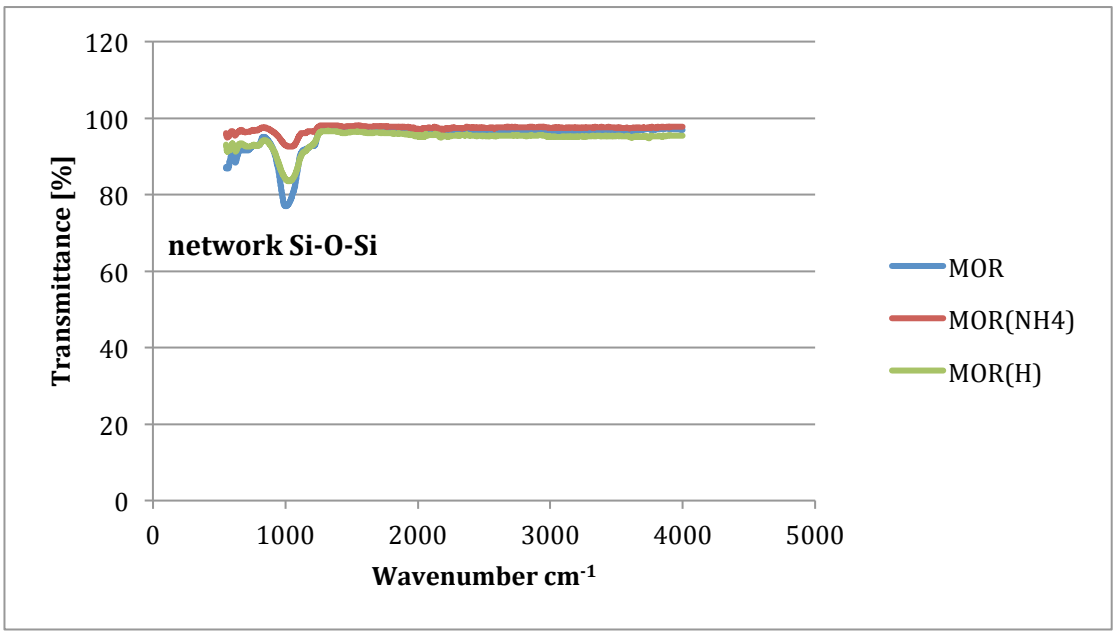

Figure 34 FT-IR of MOR, the major peaks are labeled as in the graph.

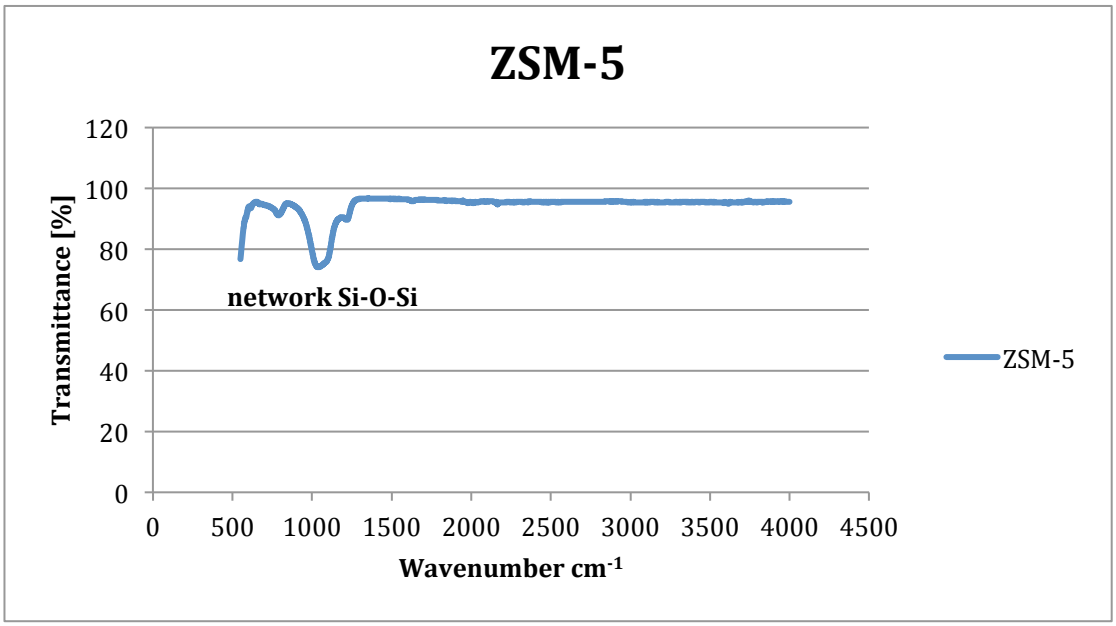

Figure 35 FT-IR of ZSM-5, the major peaks are labeled as in the graph.

From the FT-IR spectra the structures of samples do not seem to change during the ion exchange treatment. The peaks appeared in the all FT-IR spectra are $\nu^a Si-O-Si$ bonds, which represents the network of silicon and oxygen atoms in the zeolite. The C-H_2 peak emerged in the ammonia base FAU spectra means the silicon atom bonded with other content, which is ammonia in this type zeolite. Another different peak appeared uniquely is C=O peak, it indicates sediment in the samples.

4.6 BET SURFACE AREA

BET surface area was determined via gas adsorption.

Table 16 BET surface area results of zeolite sample

	Surface area (m^2/g)
Na-FAU	740.5245±17.3060
NH4-FAU	590.2058±13.4917
H-FAU	425.4243±9.3983
Na-MOR	223.1604±4.3808
NH4-MOR	190.5785±3.3226
H-MOR	152.6228±2.8024
ZSM-5	291.6197±6.7118

According to results calculated by 3Flex surface characterization analyzer, the sodium FAU has a relatively high surface area compared to other types of zeolite, which is favorable for the upgrading

reactions. According to the previous studies, the surface area of FAU is slightly higher than USY-HT500, which is another type of faujasite zeolite [44]. For the MOR and ZSM-5, they are almost the same as other studies [48]. However, with the ion exchange, the surface areas of samples decrease sharply, which was not observed in other studies. This phenomenon was not expected, since the surface area was increasing with the dealumination treatment in other researchers' work [44,48]. To explain this phenomenon, it could be caused by the squeeze of structure in FAU. With the FAU bases changed from sodium to hydrogen, the particles attaching closely, and it made a reduction of pores exposure, which located in the middle of two particles, and caused a reduction of surface areas. For MOR, the stretch of particles during the dealumination process might break pores inside of particles, which caused a decrease of surface area..

4.7 MODEL OIL HYDROGENATION

Each component of the model compound mixture (model oil) was added to a stainless batch reactor and mixed with zeolite catalyst in the reactor. Then, the reactor was sealed, pressurized with hydrogen up to and heated to the reaction temperature. After the reaction, the products were washed with chloroform, and the solvent removed on a rotary evaporator. The products were redissolved in $CDCl_3$ prior to analysis by ^1H NMR.

^1H NMR detects hydrogen atoms under different environments and as such can be used to assess the degree of reaction. The NMR spectra were compared with the original model oil. The spectrum of the model mixture prior to conversion is shown in figure 33 and figure 34.

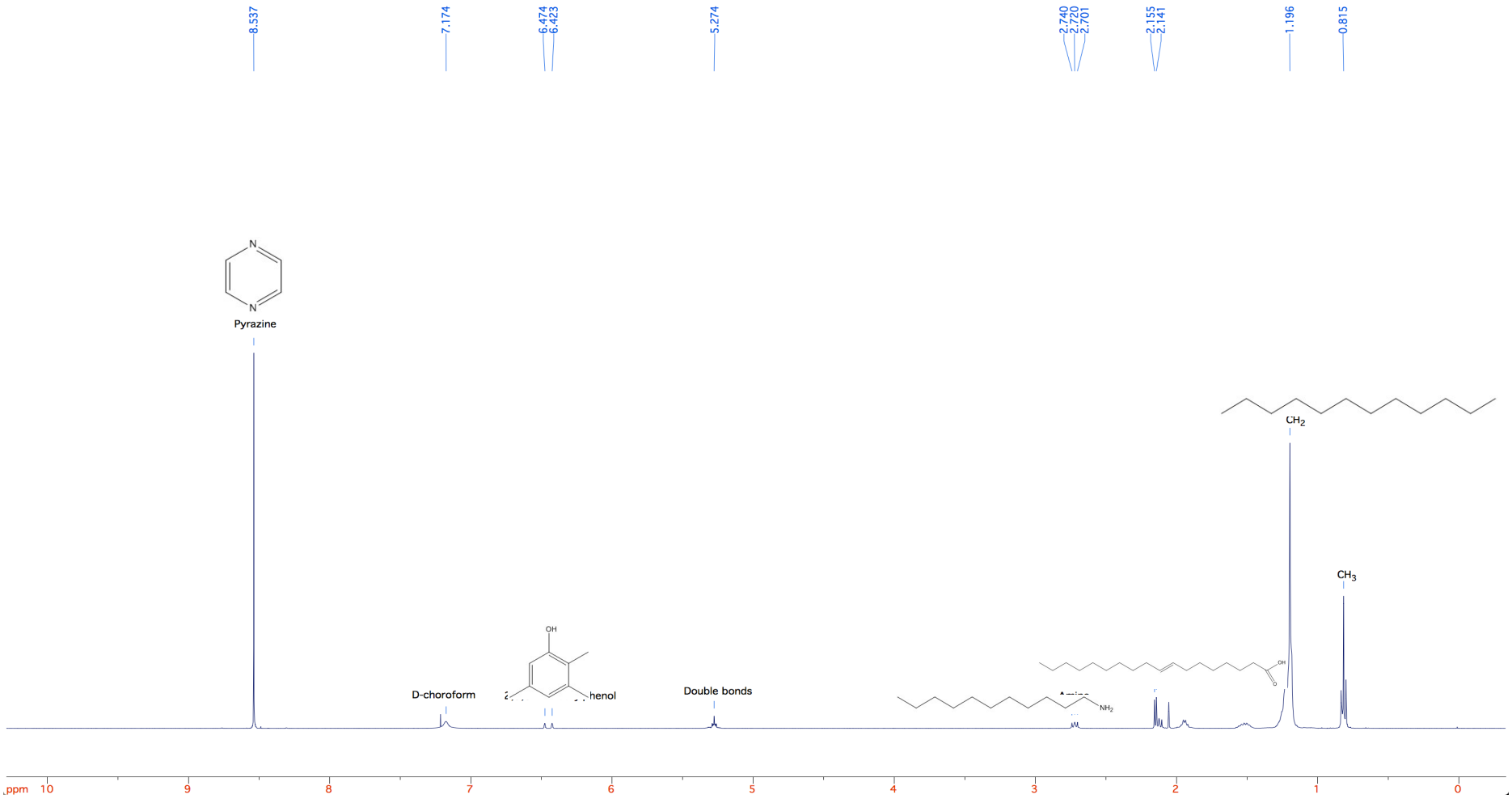

Figure 36 NMR spectrum of model mixture with D-chloroform (solvent), peaks represent α-protons of components and labeled by molecular structure of model components

Figure 37 NMR spectrum of the model mixture converted over Na-FAU with D-chloroform (solvent), peaks represent α-protons of components and labeled by molecular structure of model components

The model mixture converted over the CH_3 and CH_2 protons in the model oil fall between 0.9-1.3 ppm. These peaks will increase proportionally to the rest of the spectra as the model oil is hydrogenated. As such each peak can be compared to this region and a ratio presented to assess the degree of conversion of the molecules. The α-protons next to the amine group fall at 2.8 ppm and can be used to demonstrate the degree of denitrogenation of this molecule. In the model oil there are no peaks between 3 to 5 ppm, though some appear in the hydrogenated samples. Tentatively this could be due to the α-protons of an alcohol or other oxygenated species. Around 5.5 ppm is the peak related to the double bond protons of oleic acid, and can be used to assess the degree of hydrogenation of the samples. It should be noted that any protons bound to carbon double bonds will appear here and therefore cannot solely be used for the reduction in oleic acid. At 6.8 ppm is the peak related to the aromatic protons of 2,3,5-trimethylphenol. Finally, the aromatic protons of the pyrazine heterocycle fall at 8.7ppm and can be used to assess the degree of hydrogenation of this compound.

In order to assess the degree of reaction, the integrals of the peaks relating to the amine (2.8 ppm), the range 3-5 ppm, the double bonds (5.5 ppm), the α-protons on the oleic acid (2.3 ppm), trimethylphenol (6.8 ppm) and the pyrazine (8.7 ppm) were compared to the integrals of the CH_2 and CH_3 peaks. The change in this ratio was then assessed over the timeframe of the reaction.

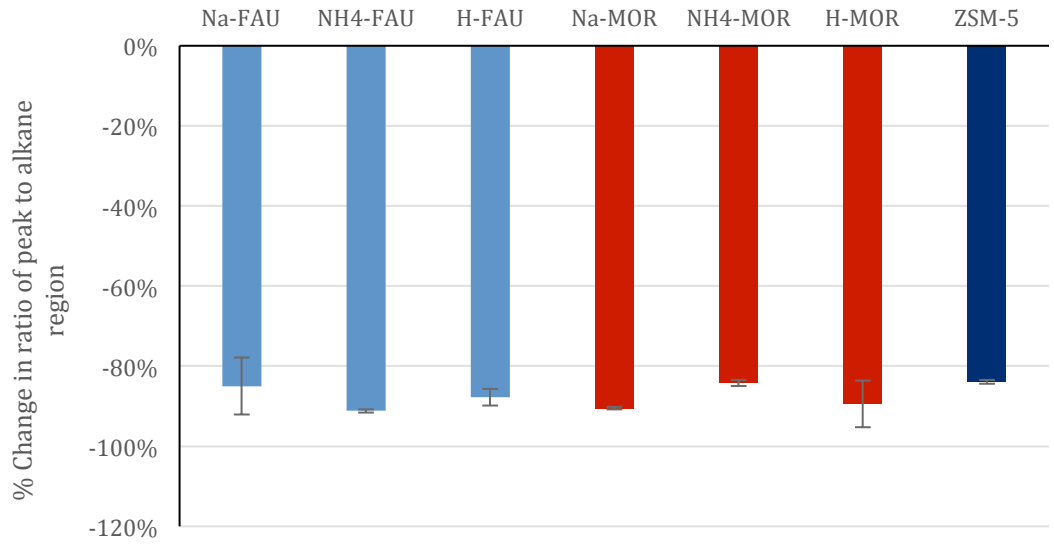

Figure 35 Percentage change in the ratio of the α-protons of dodecylamine to the alkane region (CH_3, CH_2), on reaction of the model oil at 350℃ over the zeolite catalyst

All the zeolite catalysts achieved excellent reduction of the dodecylamine with over 80% achieved. The highest activity was observed using NH_4-FAU, where the ratio between the peaks reduced by 91% after hydrogenation. Both the FAU and MOR zeolites demonstrated better performance than ZSM-5. This is presumably due to the FAU and MOR zeolites having a lower Si/Al ratio creating a more acidic environment. There is a slight advantage in using FAU zeolite over the MOR, which could be due to the higher surface area of FAU providing more catalytic sites.

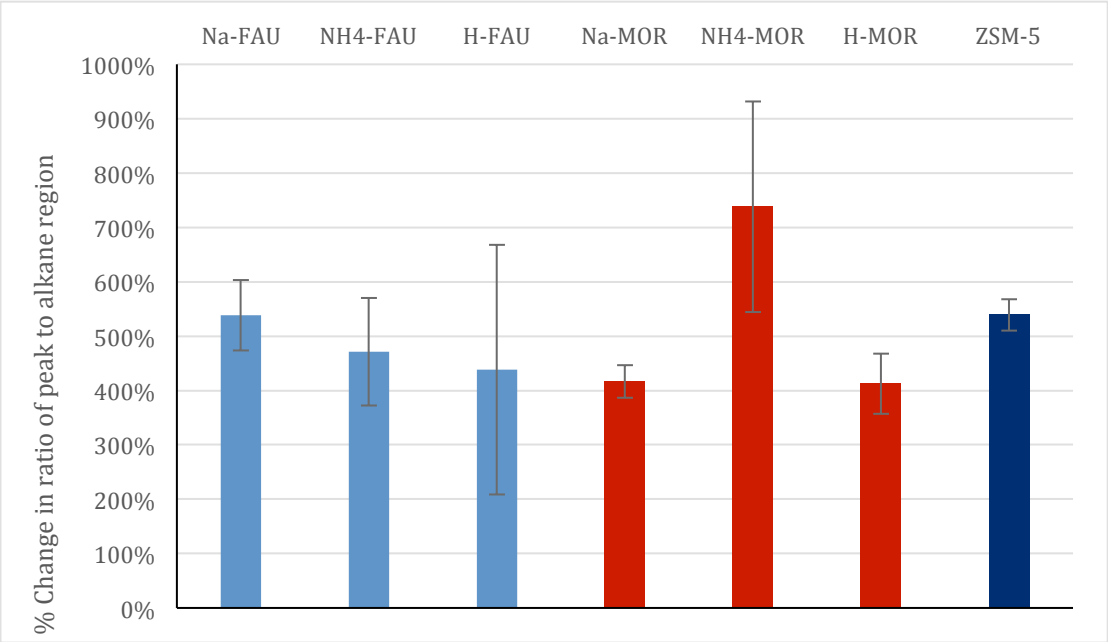

Figure 36 Percentage change in the ratio of the α-protons of 3-5 ppm range to the alkane region (CH_3, CH_2), on reaction of the model oil at 350℃ over the zeolite catalyst

With all the catalysts tested new peaks in the 3-5 ppm range were observed. This is typical of α-protons of electron withdrawing groups such as esters and alcohols. There was no statistical difference in the increase of these peaks between any of the catalysts though NH_4-MOR achieved about 740% in increase in the ratio of the integral of this region to the CH_2/CH_3 region, compared to the model oil.

According to the NMR results, there was no obvious peak in 3-5 ppm range in the model oil. Also, there were only a few tiny peaks could be observed in the oil converted over zeolite catalysts. It is possible that the products formed in this reaction are alcohols from the partial reduction of the oleic acid. MOR has the largest pore size among all the catalyst, which gives more access to absorb big size molecules like oleic acid. The lower increase of Na-MOR and H-MOR could be caused by their lower surface area, which made zeolite deactivated faster comparing to the high surface area catalysts.

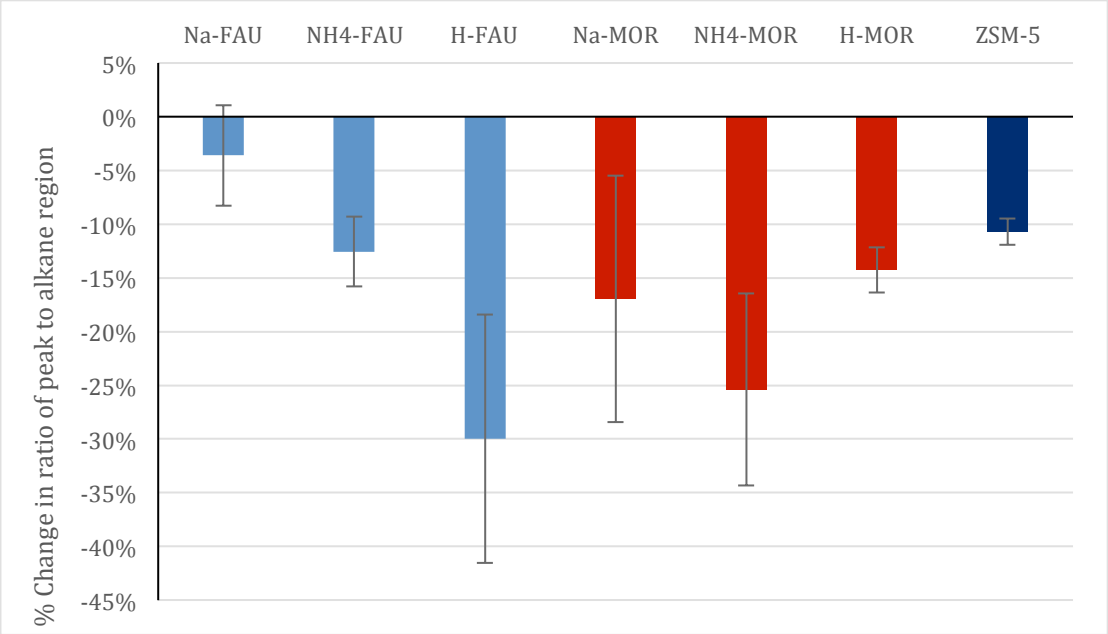

Figure 37 Percentage change in the ratio of the α-protons of oleic acid to the alkane region (CH_3, CH_2), on reaction of the model oil at 350℃ over the zeolite catalyst.

When it comes to oleic acid, all the catalysts reached reductions in a range from 4% to 30%. H-FAU achieved a 30% reduction which is the highest reduction among all catalysts. While Na-FAU done the lowest reduction about 4%. Having the lowest pore size, Na-FAU does not have a good performance on reducing the large molecules like oleic acid comparing to MOR and ZSM-5. However, with the ion exchange porcess was conducted, the active sites increase massively under a low Si/Al ratio of FAU, the performance of H-FAU was increasing sharply and up to 30% reduction. While the improvement did not appear in MOR, since it has a relatively high Si/Al ratio.

Compared with graph of 3-5 ppm range, MOR and ZSM-5 followed the increase pattern of 3-5 ppm range. However, FAU catalysts go with a contrary pattern, which may because oleic acid was degraded more completely to the alkanes comparing to MOR and ZSM-5 had more amount in alcohols and esters.

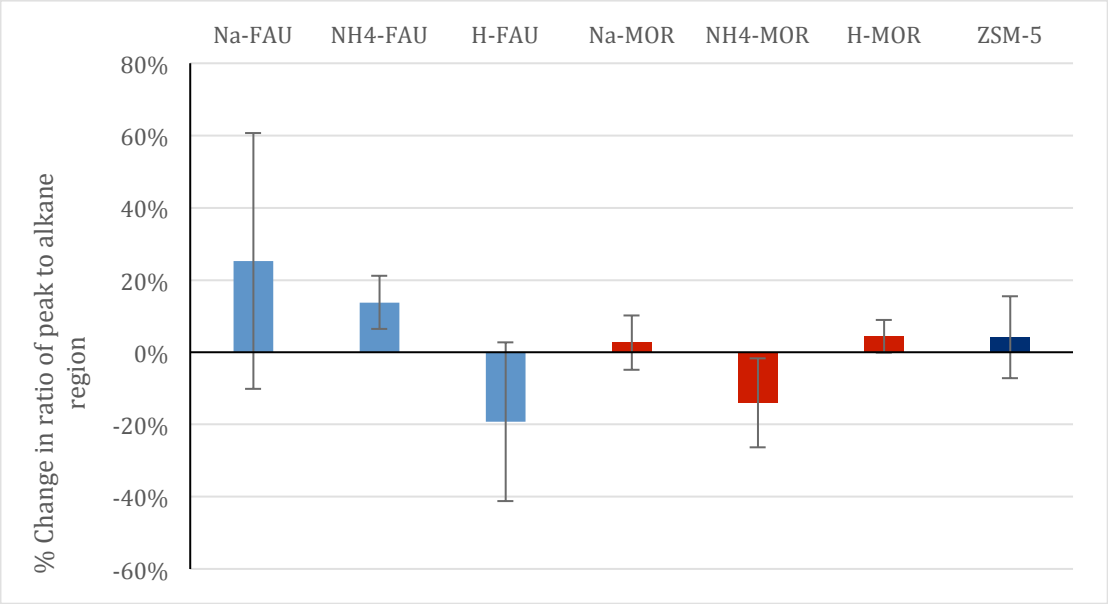

Figure 38 Percentage change in the α-protons of double bonds group to the alkane region (CH_3, CH_2), on reaction of the model oil at 350℃ over the zeolite catalyst

Interestingly, despite a reduction in the oleic acid content, the double bond region does not change dramatically. None of the FAU zeolites reduced this region, with any change in the ratio seemingly statistically insignificant. Similarly the MOR or ZSM-5 catalysts did not reduce the double bonds in the samples effectively.

Figure 39 NMR spectrum overlay of the model oil and converted over Na-FAU double bond region, black line represents model oil, red line means Na-FAU converted oil

From figure 39, it can be observed that the peaks relating to the double bonds have been shifted, which indicates that we are producing new olefinic chemicals in the reaction.

The lack of activity towards double bonds could be due to the low Si/Al ratio of the catalysts, yielding a number of acidic sites have a low acidity that could produce olefins from long chain alkanes during cracking reactions. This would mean that at the catalytic sites the reaction is hydrogen limited.

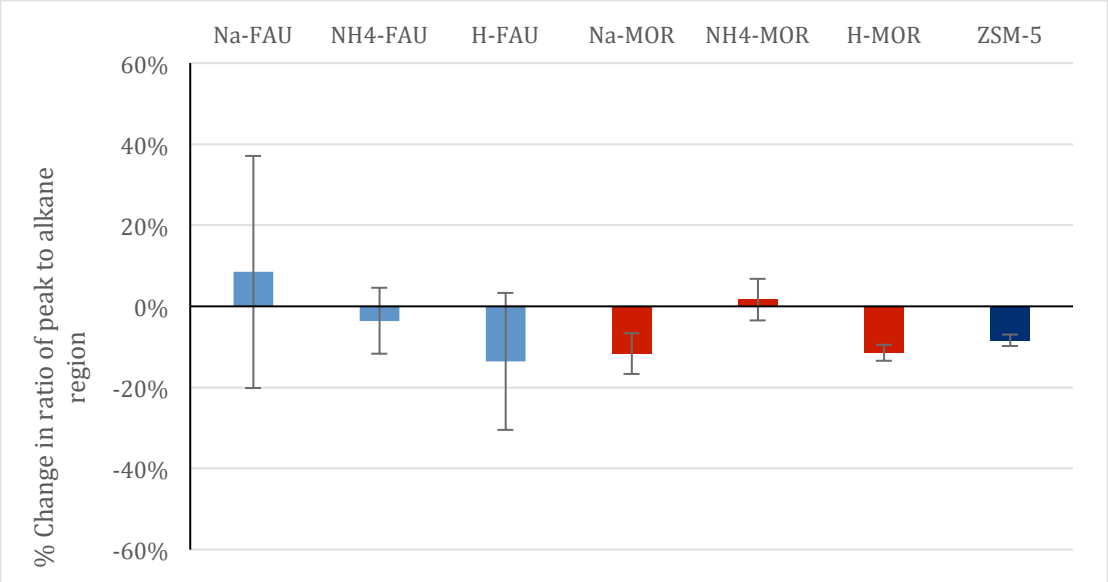

Figure 40 Percentage change in the ratio of the α-protons of trimethylphenol to the alkane region (CH_3, CH_2), on reaction of the model oil at 350℃ over the zeolite catalyst

The model oil also contained trimethylphenol, with the aim to reduce the aromatic and remove the phenol group. To examine the reduction in this molecule the peaks between 6-7 ppm in the aromatic region were used. However, similarly to the double bonds, very little activity in the hydrogenation was observed. As the FAU has small pore size and low Si/Al ratio, it is difficult to give access for trimethylphenol molecules and enough acidity to react with phenolic components. On the other hand, MOR and ZSM-5 have higher Si/Al ratio, which gives much stronger acidity than FAU, so they have higher activity on trimethylphenol.

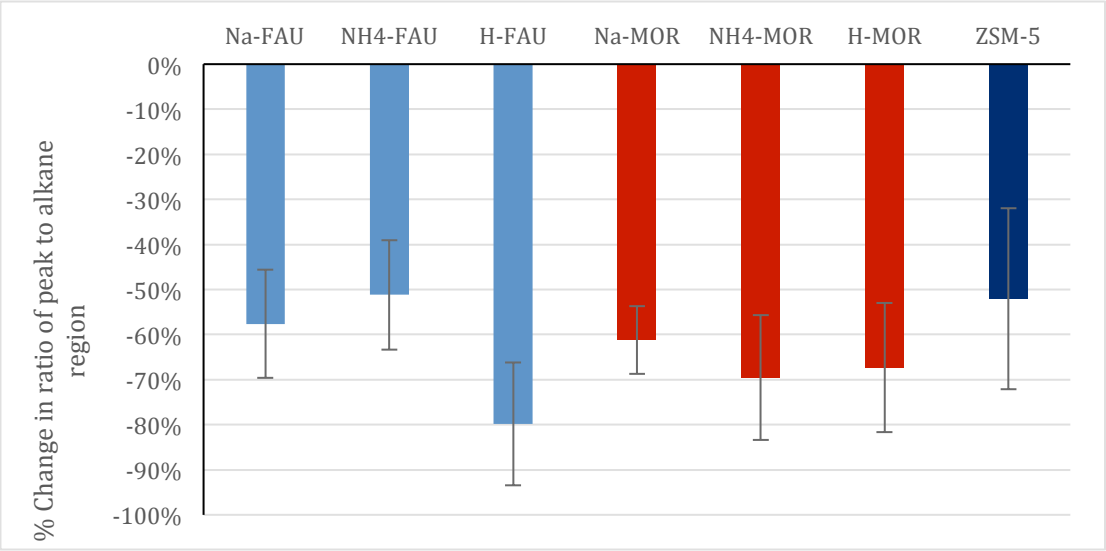

Figure 41 Percentage change in the ratio of the α-protons of pyrazine to the alkane region (CH_3, CH_2), on reaction of the model oil at 350℃ over the zeolite catalyst

Pyrazine is an aromatic hetero cycle with two nitrogen atoms. Unlike the phenol however, the catalysts screened demonstrated excellent activity for the reduction of this compound. The most effective catalyst was H-FAU, which achieved a reduction of over 80%. H-FAU has higher surface area and much lower Si/Al ratio than MOR and ZSM-5, so it has more active sites to react with pyrazine. Comparing with ZSM-5, MOR has a higher surface area and lower Si/Al ratio, this was reflected in the better performance of the MOR catalyst than ZSM-5.

According to the results above, FAU with its low Si/Al ratio and high surface area, have a higher activity comparing to the MOR and ZSM-5 in all compounds except double bonds and phenolic component, since its large amount of active sites. FAU is less active in double bonds because double bonds are mostly from large molecules, such as oleic acid, it cannot go through the small pore in the FAU. It also might because the low acidity of active sites in FAU, which could produce new double bonds in reactions. MOR and ZSM-5 have relatively high Si/Al ratio and big crystal size, which makes them have a strong acidity and easily to absorb the large molecules. However, MOR and ZSM-5 did not achieve obvious reductions in double bonds and phenolic component. It might because MOR and ZSM-5 have relatively low surface area, which could deactivate catalyst faster than normal situations.

5 CONCLUSION

Three types of zeolite; zeolite-Y (FAU), mordenite (MOR) and ZSM-5 were synthesized successfully. With a stirring ion-exchange treatment, FAU and MOR were converted from sodium base to ammonia base, this was followed by a heating process to turn the ammonia base zeolite to hydrogen base. This method was aiming to increase the active sites in the zeolite to improve their performance during the upgrading process. The zeolites that conducted ion-exchange and calcination methods were also examined by XRD respectively to ensure that the original structure was unchanged.

After the synthesis, a range of characterization methods, for instance, FT-IR, SS-NMR, SEM, BET and EDX, were used to determine the structure of the zeolite samples demonstrating that the zeolites were correct and unchanged during the modifiable process. Also, the Si/Al ratio was calculated through these characterization methods. The results show that the same type of zeolite samples in different bases have almost the same Si/Al ratio, since the dealumination and calcination processes only increase active sites in the zeolite. On the other hand, the change of T-O-T angles indicates that zeolite structure experiences a small expansion or squeeze, presumably caused by the aluminum losing. However, with zeolite dealuminating from sodium base to hydrogen base, the surface area of zeolite was also found to decrease indicating the porous structure of zeolite is reduced after the ion-exchange process. This phenomenon is different from previously reported studies.

The zeolite samples were tested as catalysts for the conversion of model oil, and the conversion assessed via ^{1}H NMR, all the zeolite samples achieved large reductions in the amine and pyrazine molecules with FAU zeolite being slightly more active than the other zeolites. However, no significant reductions in the double bond content of the phenol were observed. This demonstrates that while the zeolites can remove nitrogen effectively to produce suitable hydrocarbon fuel alternative catalysts, or further modifications of the zeolite structure are needed.

6 FUTURE WORK

As the current work only tested the zeolite catalyst with model compounds mixture, the performance and properties of testing with real bio-oil have not been studied yet. To this end, the further study can focus on testing zeolite catalyst with actual algal HTL oil. Moreover, the different reaction conditions using these catalysts also needs to be investigated, which can optimize the performance of zeolite catalyst when applies them in bio-oil upgrading, specifically by increasing the hydrogen pressure.

Alternatively, the zeolite catalyst itself could be further optimized to make it more feasible for the bio-oil upgrading process. To improve the capabilities of catalysts, there are a number of methods that can be used, such as loading noble metal particles and dealumination. The zeolite catalyst can be applied for a further dealumination to remove the aluminum extensively, which can increase the acidity of the catalyst and give the catalyst more active sites. It also can change the structure of zeolite particles. Introducing these catalysts in the upgrading process will be a new feature in this experiment. Loading noble metals, for instance, platinum is another method to improve the performance of catalyst in bio-oil upgrading process. Loading noble metals on zeolites synthesized in this project and testing them on both the model oil and the HTL oil would demonstrate the increase in activity.

It is also necessary to simplify the synthesize methods and yield of zeolite samples. For example, the mordenite in this project is very difficult to synthesize with a large yield, since the volume of stainless autoclave restricts the yield of mordenite in one batch. The purity of mordenite is also not ideal in this project. Therefore, optimizing the current recipe of zeolite synthesis is also a critical factor in bio-oil upgrading process. An improvement of synthesizes methods and yield can provide more amounts of catalysts during the experiment, shorten the upgrading reaction period and obtain a more accurate result.

7 REFERENCES

1. Villadsen, S.R., L. Dithmer, R. Forsberg, J. Becker, A. Rudolf, S.B. Iversen, B.B. Iversen, and M. Glasius, *Development and Application of Chemical Analysis Methods for Investigation of Bio-Oils and Aqueous Phase from Hydrothermal Liquefaction of Biomass.* Energy & Fuels, 2012: p. 6988-6998.
2. Chen, W.H., B.J. Lin, M.Y. Huang, and J.S. Chang, *Thermochemical conversion of microalgal biomass into biofuels: A review.* Bioresour Technol, 2015. **184**: p. 314-327.
3. Baeyens, J., Q. Kang, L. Appels, R. Dewil, Y. Lv, and T. Tan, *Challenges and opportunities in improving the production of bio-ethanol.* Progress in Energy and Combustion Science, 2015. **47**(0): p. 60-88.
4. Tian, Y., L. Zhao, H. Meng, L. Sun, and J. Yan, *Estimation of un-used land potential for biofuels development in (the) People's Republic of China.* Applied Energy, 2009. **86, Supplement 1**(0): p. S77-S85.
5. Kang, S., X. Li, J. Fan, and J. Chang, *Hydrothermal conversion of lignin: A review.* Renewable and Sustainable Energy Reviews, 2013. **27**: p. 546-558.
6. Singh, R., B. Balagurumurthy, and T. Bhaskar, *Hydrothermal liquefaction of macro algae: Effect of feedstock composition.* Fuel, 2015. **146**: p. 69-74.
7. Miao, X., Q. Wu, and C. Yang, *Fast pyrolysis of microalgae to produce renewable fuels.* Journal of Analytical and Applied Pyrolysis, 2004. **71**(2): p. 855-863.
8. Allen, E., D.M. Wall, C. Herrmann, A. Xia, and J.D. Murphy, *What is the gross energy yield of third generation gaseous biofuel sourced from seaweed?* Energy, 2015. **81**(0): p. 352-360.
9. Pragya, N., K.K. Pandey, and P.K. Sahoo, *A review on harvesting, oil extraction and biofuels production technologies from microalgae.* Renewable and Sustainable Energy Reviews, 2013. **24**: p. 159-171.
10. Chen, W., Z. Luo, C. Yu, G. Li, Y. Yang, and H. Zhang, *Upgrading of bio-oil in supercritical ethanol: Catalysts screening, solvent recovery and catalyst stability study.* The Journal of Supercritical Fluids, 2014. **95**: p. 387-393.
11. Zhu, Y., M.J. Biddy, S.B. Jones, D.C. Elliott, and A.J. Schmidt, *Techno-economic analysis of liquid fuel production from woody biomass via hydrothermal liquefaction (HTL) and upgrading.* Applied Energy, 2014. **129**(0): p. 384-394.
12. Chen, W., Z. Luo, C. Yu, G. Li, Y. Yang, J. Zhang, and K. Lu, *Catalytic transformations of acids, aldehydes, and phenols in bio-oil to alcohols and esters.* Fuel, 2014. **135**: p. 55-62.
13. Bridgwater, A.V., *Production of high grade fuels and chemicals from*

catalytic pyrolysis of biomass. Catalysis today, 1996. **29**(1-4): p. 285-295.
14. Zhang, J. and Y. Zhang, *Hydrothermal Liquefaction of Microalgae in an Ethanol–Water Co-Solvent To Produce Biocrude Oil.* Energy & Fuels, 2014. **28**(8): p. 5178-5183.
15. Tian, C., B. Li, Z. Liu, Y. Zhang, and H. Lu, *Hydrothermal liquefaction for algal biorefinery: A critical review.* Renewable and Sustainable Energy Reviews, 2014. **38**: p. 933-950.
16. Demirbas, A., *Competitive liquid biofuels from biomass.* Applied Energy, 2011. **88**(1): p. 17-28.
17. Xu, C. and N. Lad, *Production of Heavy Oils with High Caloric Values by Direct Liquefaction of Woody Biomass in Sub/Near-critical Water.* Energy & fuels, 2008. **22**(1): p. 635-642.
18. *Hydrothermal liquefaction -- the most promising path to a sustainable bio-oil production*. 2013; Available from: http://www.eurekalert.org/multimedia/pub/52593.php.
19. Elliott, D., *Historical Developments in Hydroprocessing Bio-oils.* Energy & fuels, 2007. **21**(3): p. 1792-1815.
20. Adjaye, J.D. and N.N. Bakhshi, *Catalytic conversion of a biomass-derived oil to fuels and chemicals I: Model compound studies and reaction pathways.* Biomass and Bioenergy, 1995. **8**(3): p. 131-149.
21. Adjaye, J.D. and N.N. Bakhshi, *Production of hydrocarbons by catalytic upgrading of a fast pyrolysis bio-oil. Part I: Conversion over various catalysts.* Fuel Processing Technology, 1995. **45**(3): p. 161-183.
22. Wildschut, J., F.H. Mahfud, R.H. Venderbosch, and H.J. Heeres, *Hydrotreatment of fast pyrolysis oil using heterogeneous noble-metal catalysts.* Industrial and Engineering Chemistry Research, 2009. **48**(23): p. 10324-10334.
23. Mortensen, P.M., J.D. Grunwaldt, P.A. Jensen, K.G. Knudsen, and A.D. Jensen, *A review of catalytic upgrading of bio-oil to engine fuels.* Applied Catalysis A: General, 2011. **407**(1–2): p. 1-19.
24. Venderbosch, R.H., A.R. Ardiyanti, J. Wildschut, A. Oasmaa, and H.J. Heeres, *Stabilization of biomass-derived pyrolysis oils.* Journal of Chemical Technology & Biotechnology, 2010. **85**(5): p. 674-686.
25. Tan, Z., X. Xu, Y. Liu, C. Zhang, Y. Zhai, P. liu, Y. Li, and R. Zhang, *Upgrading bio-oil model compounds phenol and furfural within situgenerated hydrogen.* Environmental Progress & Sustainable Energy, 2014. **33**(3): p. 751-755.
26. de Miguel Mercader, F., M.J. Groeneveld, S.R.A. Kersten, N.W.J. Way, C.J. Schaverien, and J.A. Hogendoorn, *Production of advanced biofuels: Co-processing of upgraded pyrolysis oil in standard refinery units.* Applied Catalysis B: Environmental, 2010. **96**(1-2): p. 57-66.
27. Duan, P., B. Wang, and Y. Xu, *Catalytic hydrothermal upgrading of crude*

bio-oils produced from different thermo-chemical conversion routes of microalgae. Bioresource Technology, 2015. **186**(0): p. 58-66.
28. Sanna, A., T.P. Vispute, and G.W. Huber, *Hydrodeoxygenation of the aqueous fraction of bio-oil with Ru/C and Pt/C catalysts.* Applied Catalysis B: Environmental, 2015. **165**: p. 446-456.
29. Elliott, D.C. and T.R. Hart, *Catalytic Hydroprocessing of Chemical Models for Bio-oil.* Energy & Fuels, 2009. **23**(2): p. 631-637.
30. Veses, A., B. Puértolas, M.S. Callén, and T. García, *Catalytic upgrading of biomass derived pyrolysis vapors over metal-loaded ZSM-5 zeolites: Effect of different metal cations on the bio-oil final properties.* Microporous and Mesoporous Materials, 2015. **209**(0): p. 189-196.
31. Pham, T.N., D. Shi, and D.E. Resasco, *Evaluating strategies for catalytic upgrading of pyrolysis oil in liquid phase.* Applied Catalysis B: Environmental, 2014. **145**: p. 10-23.
32. Lappas, A.A., S. Bezergianni, and I.A. Vasalos, *Production of biofuels via co-processing in conventional refining processes.* Catalysis Today, 2009. **145**(1-2): p. 55-62.
33. Butler, E., G. Devlin, D. Meier, and K. McDonnell, *A review of recent laboratory research and commercial developments in fast pyrolysis and upgrading.* Renewable and Sustainable Energy Reviews, 2011. **15**(8): p. 4171-4186.
34. Vermeiren, W. and J.P. Gilson, *Impact of Zeolites on the Petroleum and Petrochemical Industry.* Topics in Catalysis, 2009. **52**(9): p. 1131-1161.
35. Zhang, C., J. Xing, L. Song, H. Xin, S. Lin, L. Xing, and X. Li, *Aqueous-phase hydrodeoxygenation of lignin monomer eugenol: Influence of Si/Al ratio of HZSM-5 on catalytic performances.* Catalysis Today, 2014. **234**: p. 145-152.
36. van Donk, S., J.H. Bitter, A. Verberckmoes, M. Versluijs-Helder, A. Broersma, and K.P. de Jong, *Physicochemical Characterization of Porous Materials: Spatially Resolved Accessibility of Zeolite Crystals.* Angewandte Chemie, 2005. **117**(9): p. 1384-1387.
37. Chal, R., C. Gérardin, M. Bulut, and S. van Donk, *Overview and Industrial Assessment of Synthesis Strategies towards Zeolites with Mesopores.* ChemCatChem, 2011. **3**(1): p. 67-81.
38. Hriljac, J.A., M.M. Eddy, A.K. Cheetham, J.A. Donohue, and G.J. Ray, *Powder Neutron Diffraction and 29Si MAS NMR Studies of Siliceous Zeolite-Y.* Journal of Solid State Chemistry, 1993. **106**(1): p. 66-72.
39. (IZA), T.I.Z.A. *FAU*. Available from: http://izasc.ethz.ch/fmi/xsl/IZA-SC/ftc_fw.xsl?-db=Atlas_main&-lay=fw&STC=FAU&-find.
40. Agudelo, J.L., E.J.M. Hensen, S.A. Giraldo, and L.J. Hoyos, *Influence of steam-calcination and acid leaching treatment on the VGO hydrocracking*

performance of faujasite zeolite. Fuel Processing Technology, 2015. **133**: p. 89-96.
41. Samanta, S., N.K. Mal, P. Kumar, and A. Bhaumik, *Hydrothermally synthesized high silica mordenite as an efficient catalyst in alkylation reaction under liquid phase condition.* Journal of Molecular Catalysis A: Chemical, 2004. **215**(1-2): p. 169-175.
42. (IZA), T.I.Z.A. *MOR*. Available from: http://izasc.biw.kuleuven.be/fmi/xsl/IZA-SC/ftc_fw.xsl?-db=Atlas_main&-lay=fw&-max=25&STC=MOR&-find.
43. Lin, J.-S., J.-J. Wang, J. Wang, I. Wang, R.J. Balasamy, A. Aitani, S. Al-Khattaf, and T.-C. Tsai, *Catalysis of alkaline-modified mordenite for benzene alkylation of diolefin-containing dodecene for linear alkylbenzene synthesis.* Journal of Catalysis, 2013. **300**: p. 81-90.
44. Boveri, M., C. Márquez-Álvarez, M.Á. Laborde, and E. Sastre, *Steam and acid dealumination of mordenite.* Catalysis Today, 2006. **114**(2-3): p. 217-225.
45. Čejka, J. and H. van Bekkum, *Zeolites and Ordered Mesoporous Materials: Progress and Prospects : the 1st FEZA School on Zeolites, Prague, Czech Republic, August 20-21, 2005*. 2005: Elsevier.
46. (IZA), T.I.Z.A. *MFI*. Available from: http://izasc.ethz.ch/fmi/xsl/IZA-SC/ftc_fw.xsl?-db=Atlas_main&-lay=fw&-max=25&STC=MFI&-find.
47. Vichaphund, S., D. Aht-ong, V. Sricharoenchaikul, and D. Atong, *Production of aromatic compounds from catalytic fast pyrolysis of Jatropha residues using metal/HZSM-5 prepared by ion-exchange and impregnation methods.* Renewable Energy, 2015. **79**(0): p. 28-37.
48. Lu, Q., Z.-F. Zhang, C.-Q. Dong, and X.-F. Zhu, *Catalytic Upgrading of Biomass Fast Pyrolysis Vapors with Nano Metal Oxides: An Analytical Py-GC/MS Study.* Energies, 2010. **3**(11): p. 1805-1820.
49. Rutkowska, M., Z. Piwowarska, E. Micek, and L. Chmielarz, *Hierarchical Fe-, Cu- and Co-Beta zeolites obtained by mesotemplate-free method. Part I: Synthesis and catalytic activity in N2O decomposition.* Microporous and Mesoporous Materials, 2015. **209**: p. 54-65.
50. Groen, J.C., S. Abelló, L.A. Villaescusa, and J. Pérez-Ramírez, *Mesoporous beta zeolite obtained by desilication.* Microporous and Mesoporous Materials, 2008. **114**(1-3): p. 93-102.
51. Omegna, A., M. Vasic, J. Anton van Bokhoven, G. Pirngruber, and R. Prins, *Dealumination and realumination of microcrystalline zeolite beta: an XRD, FTIR and quantitative multinuclear (MQ) MAS NMR study.* Physical Chemistry Chemical Physics, 2004. **6**(2): p. 447.
52. Carvalho, K.T.G. and E.A. Urquieta-Gonzalez, *Microporous–mesoporous ZSM-12 zeolites: Synthesis by using a soft template and textural, acid and*

catalytic properties. Catalysis Today, 2015. **243**(0): p. 92-102.
53. Corma, A., U. Diaz, V. Fornés, J.M. Guil, J. Martínez-Triguero, and E.J. Creyghton, *Characterization and catalytic activity of MCM-22 and MCM-56 compared with ITQ-2.* Journal of Catalysis, 2000. **191**(1): p. 218-224.
54. Xing, C., G. Yang, M. Wu, R. Yang, L. Tan, P. Zhu, Q. Wei, J. Li, J. Mao, Y. Yoneyama, and N. Tsubaki, *Hierarchical zeolite Y supported cobalt bifunctional catalyst for facilely tuning the product distribution of Fischer–Tropsch synthesis.* Fuel, 2015. **148**: p. 48-57.
55. ETH. *Bragg's Law of Diffraction*. Available from: http://www.microscopy.ethz.ch/bragg.htm.
56. Patterson, A.L., *The Scherrer Formula for X-Ray Particle Size Determination.* Physical Review, 1939. **56**(10): p. 978-982.
57. Linser, R., U. Fink, and B. Reif, *Proton-detected scalar coupling based assignment strategies in MAS solid-state NMR spectroscopy applied to perdeuterated proteins.* Journal of Magnetic Resonance, 2008. **193**(1): p. 89-93.
58. Gullion, T. and J. Schaefer, *Rotational-echo double-resonance NMR.* Journal of Magnetic Resonance, 2011. **213**(2): p. 413-417.
59. Schanda, P., B.H. Meier, and M. Ernst, *Quantitative Analysis of Protein Backbone Dynamics in Microcrystalline Ubiquitin by Solid-State NMR Spectroscopy.* Journal of the American Chemical Society, 2010. **132**(45): p. 15957-15967.
60. Liu, Y., H. Nekvasil, and J. Tossell, *Explaining the Effects of T–O–T Bond Angles on NMR Chemical Shifts in Aluminosilicates: A Natural Bonding Orbital (NBO) and Natural Chemical Shielding (NCS) Analysis.* The Journal of Physical Chemistry A, 2005. **109**(13): p. 3060-3066.
61. Mintova, S., V. Valtchev, T. Onfroy, C. Marichal, H. Knözinger, and T. Bein, *Variation of the Si/Al ratio in nanosized zeolite Beta crystals.* Microporous and Mesoporous Materials, 2006. **90**(1-3): p. 237-245.
62. Horisberger, M., *Colloidal gold : a cytochemical marker for light and fluorescent microscopy and for transmission and scanning electron microscopy.* Scanning electron microscopy, 1981(Pt 2): p. 9-31.
63. Goldstein, J., *Scanning Electron Microscopy and X-ray Microanalysis: Third Edition*. 2003: Springer US.
64. Connes, J. and P. Connes, *Near-Infrared Planetary Spectra by Fourier Spectroscopy. I. Instruments and Results.* Journal of the Optical Society of America, 1966. **56**(7): p. 896-910.
65. Brunauer, S., P.H. Emmett, and E. Teller, *Adsorption of Gases in Multimolecular Layers.* Journal of the American Chemical Society, 1938. **60**(2): p. 309-319.
66. *Chapter 46 - FAU Linde Type Y Si(71), Al(29)*, in *Verified Syntheses of Zeolitic Materials*, H. Robson and K.P. Lillerud, Editors. 2001, Elsevier

Science: Amsterdam. p. 156-158.
67. *Chapter 68 - MOR Mordenite Si(90), Al(10)*, in *Verified Syntheses of Zeolitic Materials*, H. Robson and K.P. Lillerud, Editors. 2001, Elsevier Science: Amsterdam. p. 212-213.
68. *Chapter 62 - MFI High-Alumina ZSM-5 Si(93), Al(7)*, in *Verified Syntheses of Zeolitic Materials*, H. Robson and K.P. Lillerud, Editors. 2001, Elsevier Science: Amsterdam. p. 198-200.
69. Dyer, A., *Chapter 14 - Ion exchange capacity*, in *Verified Syntheses of Zeolitic Materials*, H. Robson and K.P. Lillerud, Editors. 2001, Elsevier Science: Amsterdam. p. 67-68.
70. *UnitCell*. Available from: http://www.ccp14.ac.uk/ccp/web-mirrors/crush/astaff/holland/UnitCell.html.
71. Milina, M., S. Mitchell, and J. Pérez-Ramírez, *Prospectives for bio-oil upgrading via esterification over zeolite catalysts.* Catalysis Today, 2014. **235**: p. 176-183.
72. Treacy, M.M.J. and J.B. Higgins, *FAU - Faujasite*, in *Collection of Simulated XRD Powder Patterns for Zeolites (fifth)*, M.M.J. Treacy and J.B. Higgins, Editors. 2007, Elsevier Science B.V.: Amsterdam. p. 166-167.
73. Treacy, M.M.J. and J.B. Higgins, *MOR - Mordenite*, in *Collection of Simulated XRD Powder Patterns for Zeolites (fifth)*, M.M.J. Treacy and J.B. Higgins, Editors. 2007, Elsevier Science B.V.: Amsterdam. p. 284-285.
74. Treacy, M.M.J. and J.B. Higgins, *MFI - ZSM-5, Calcined*, in *Collection of Simulated XRD Powder Patterns for Zeolites (fifth)*, M.M.J. Treacy and J.B. Higgins, Editors. 2007, Elsevier Science B.V.: Amsterdam. p. 278-279.
75. Burton, A.W., K. Ong, T. Rea, and I.Y. Chan, *On the estimation of average crystallite size of zeolites from the Scherrer equation: A critical evaluation of its application to zeolites with one-dimensional pore systems.* Microporous and Mesoporous Materials, 2009. **117**(1–2): p. 75-90.